

## THE SUPPLY-GENERATED SEQUENCE: A UNIFIED SEQUENCE-STRATIGRAPHIC MODEL FOR CLOSED LACUSTRINE SEDIMENTARY BASINS WITH EVIDENCE FROM THE GREEN RIVER FORMATION, UNTA BASIN, UTAH, U.S.A.

JAMES H. GEARON,<sup>1,2</sup> CORNEL OLARIU,<sup>2,3</sup> AND RONALD J. STEEL<sup>2</sup>

<sup>1</sup>Department of Earth and Atmospheric Sciences, Indiana University, 1001 East 10th Street, Bloomington, Indiana 47408, U.S.A.

<sup>2</sup>Department of Geological Sciences, Jackson School of Geosciences, University of Texas at Austin, 23 San Jacinto Boulevard, Austin, Texas 78712, U.S.A.

<sup>3</sup>National Institute for Marine Geology and Geoecology, 23-25 Dimitrie Onciu Street, Bucharest 024053, Romania

e-mail: jhgearon@iu.edu

**ABSTRACT:** Closed lakes and oceans are stratigraphically distinct systems. However, closed-lake stratigraphy is often interpreted using conventional sequence stratigraphic concepts which were generated for marine settings. As a consequence, lacustrine stratigraphy has long been vexing and applied on an ad-hoc basis. To remedy this, we present a novel, unified sequence stratigraphic model for hydrologically closed (endorheic) basins: the Supply-Generated Sequence (SGS) Model. This model was generated to interpret our outcrop-based correlation—the largest to date at ~ 30 km—across the Sunnyside Interval member of the middle Green River Formation in Nine Mile Canyon near Price, Utah, USA. The SGS model is based on the fundamental sedimentological and hydrodynamic differences between closed lakes and marine settings wherein the relationship between water discharge and sediment discharge is highly correlated. The SGS model divides packages of genetic lacustrine strata by bounding correlative surfaces, conformable or unconformable, separating facies and surfaces associated with low clastic supply (e.g., carbonates, mudstones, or exposure surfaces) from facies characteristic of relatively higher amounts of clastic supply (subaerial channelized sandstones, subaqueous siltstones, and pedogenic mudstones). We use the SGS model to correlate regional sequences at a higher resolution than previous interpretations and find the greatest amount of clastic deposition occurs during periods of lake-level rise, indicating that the SGSs are characteristically transgressive. Additionally, this model removes the implicit and explicit base-level assumptions of previous sequence stratigraphic models while being agnostic to the source of increased sediment discharge and therefore generalizable to other closed lacustrine settings. We use the high-resolution supply-generated sequences (meters thick) to argue for a climatic origin of the cyclic Sunnyside interval deposits based on sequence durations (40–50 kyr), and aligning sequences with recognized early Eocene transitory hyperthermal event timing and their associated climatic shifts across the region, increasing riverine discharge of sediment and water.

### INTRODUCTION

Closed lacustrine sedimentary systems remain enigmatic in the stratigraphic record. While strides have been made in analysis of siliciclastic shallow (Overeem et al. 2003; Hoogendoorn et al. 2005; Jorissen et al. 2020), deep (Fongnern et al. 2018; Balázs et al. 2018), and mixed siliciclastic–carbonate (Tänavsuu–Milkeviciene et al. 2017) lacustrine basins, regional stratigraphy of lacustrine deposits in fold–thrust-belt systems (DeCelles and Giles 1996; Carroll and Bohacs 1999; Horton et al. 2002; Lawton 2019), and basin-fill facies models (Carroll and Bohacs 1999; Bohacs et al. 2000), deciphering local, single delta-scale sedimentation patterns of closed, continental lacustrine systems remains difficult. This challenge arises from their limited representation in the stratigraphic record (Laske 1997) and the application of marine-based techniques such as sequence stratigraphy to deposits decoupled from eustasy. The very different timescales at which marine and lacustrine base levels oscillate further complicate the stratigraphic record and make interpretation complex, often

forcing the geologist to deal with multiple time-transgressive, high-frequency cycles that may be preserved or removed by later erosion. The Green River Formation of the Laramide intermontane basins (Fig. 1) serves as proof of this difficulty. These basins were filled with long-lived lakes throughout the early Paleogene (Dickinson and Snyder 1978). While the lakes have aided in large, synoptic reconstructions of Sevier–Laramide interactions (Smith et al. 2008; Fan and Carrapa 2014; Lawton 2019), high-resolution studies of closed lacustrine depositional systems often disagree on the nature of event-scale sediment delivery to these basins (Jacob 1969; Ryder et al. 1976; Remy 1991; Keighley et al. 2002; Pusca 2004; Taylor and Ritts 2004; Schomacker et al. 2010; Moore et al. 2012; Gall et al. 2017; Birgenheier et al. 2020; Wang and Plink-Björklund 2020). To address these discrepancies, a high-resolution, 30 km cross section through 10 newly defined stratigraphic supply-generated sequences (SGSs) along the southern margin of Uinta Basin from Nine Mile Canyon in Utah, USA (Figs. 1, 2) is presented. This outcrop correlation is, to our knowledge, the most detailed known collation of field-measured data for this stratigraphic interval.

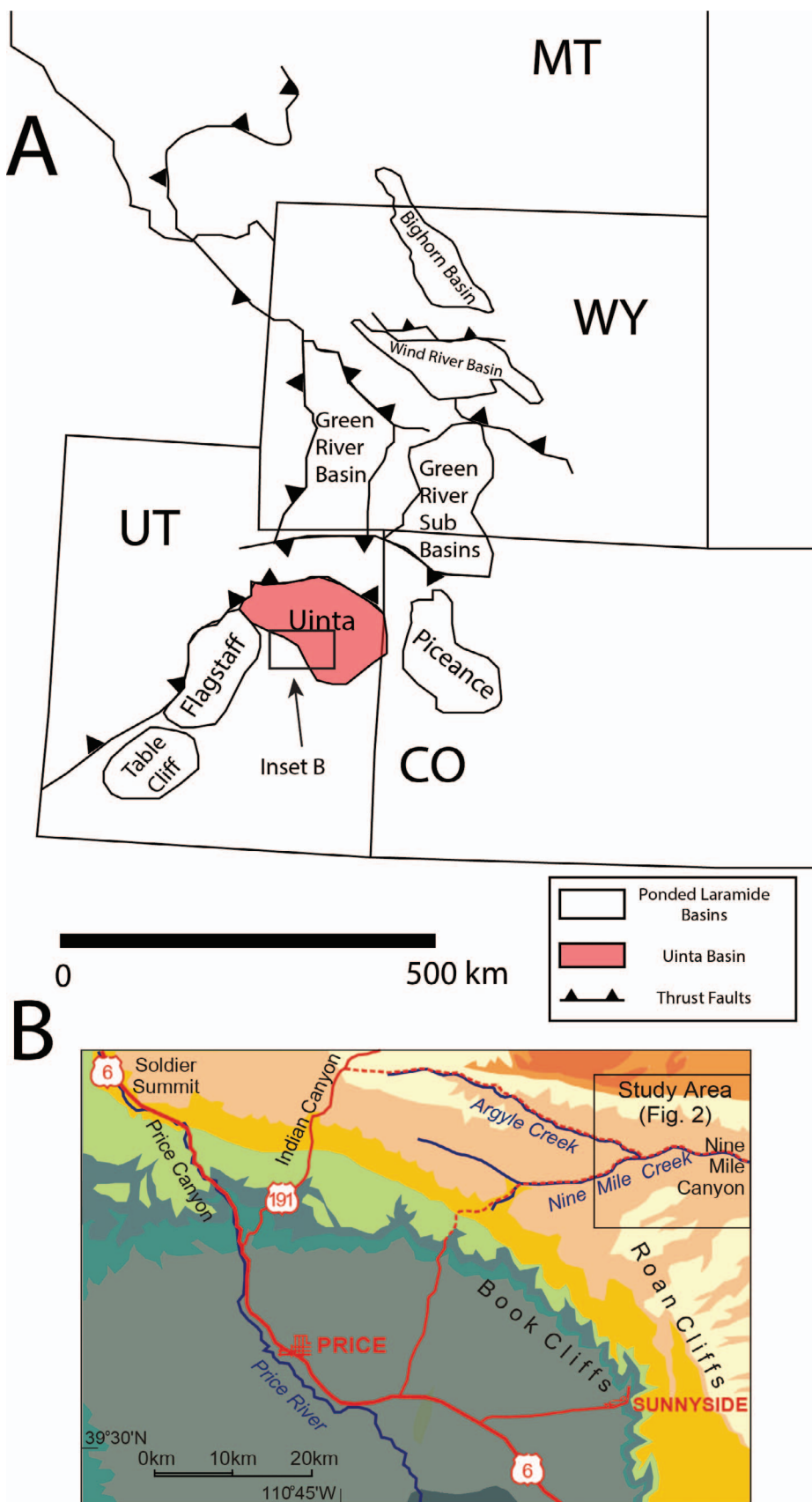


FIG. 1.—Tectonic and Stratigraphic overview of the **A**) Laramide intermontane basins (modified from Lawton 2019). **B**) Regional stratigraphic map of the Uinta Basin (modified from Keighley et al. 2002).

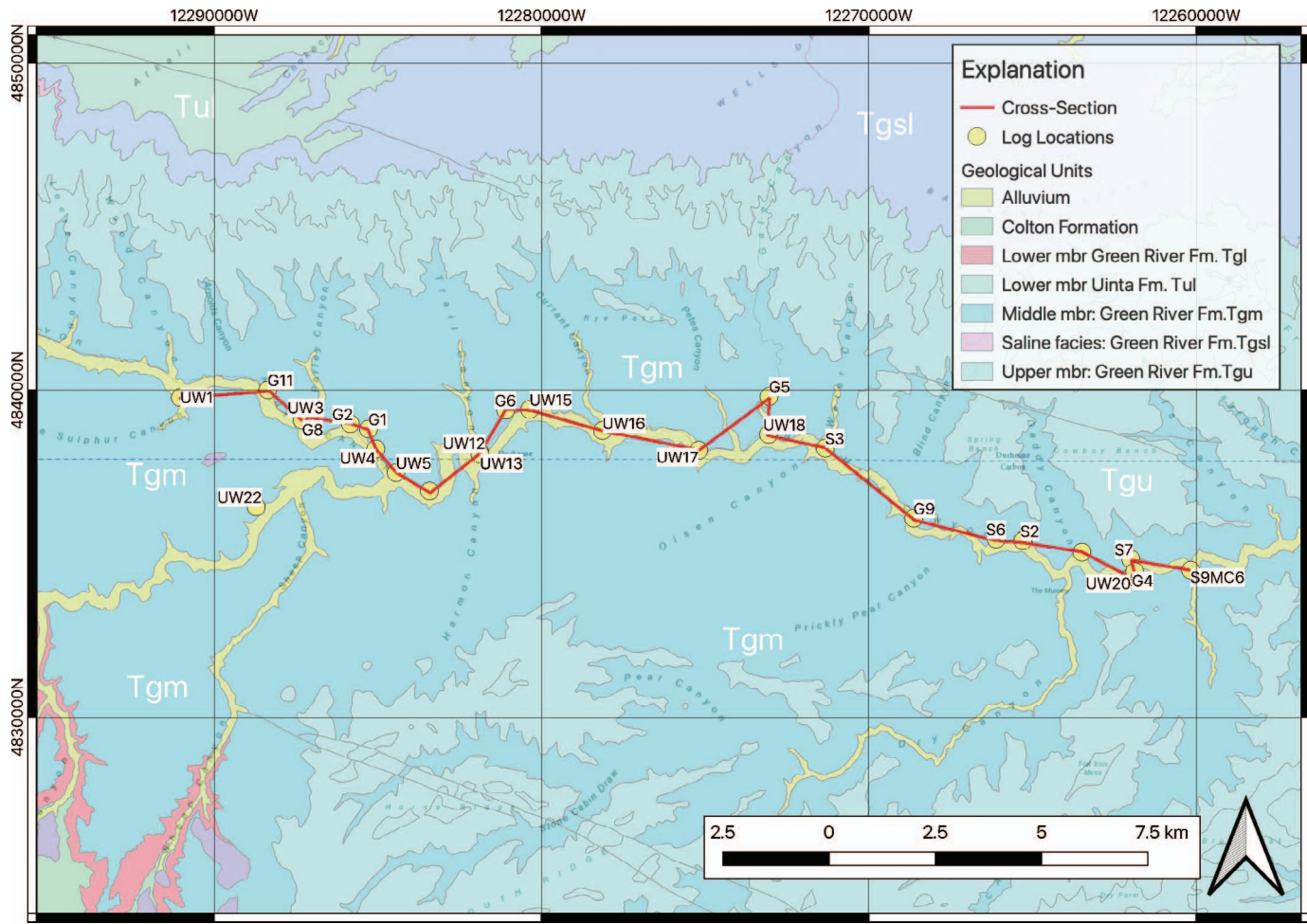


FIG. 2.—Geologic Map of study area: Nine Mile and Argyle Canyons NE of Price, Utah. Geologic map units and log locations are shown. Coordinates are in UTM WGS84.

### Scope

We utilize the pristine exposures of tens of kilometers of outcrop of the Eocene Green River Formation in Nine Mile Canyon, Uinta Basin, Utah, to advance scientific understanding of shallow-water clastic and carbonate deposits in paleo-lakes through a framework for identifying cyclic fluvio-lacustrine deposits in outcrop exposures. Using previous published stratigraphic sections combined with new, bed-scale observations, 10 lacustrine supply-generated sequences (defined in this study) are described, with emphasis on intra-sequence channel architecture (bed geometries, facies) and overall sequence architecture. The results point to a regular (and predictable) alternation of lithologies in the proposed SGSSs, consistent with their transgressive (rising lake level) character due to the coupling of sediment and water influx during periods of sediment dispersal, remobilization, and deposition (a pattern discussed in detail below). SGSSs show characteristic, highly variable internal bedding geometry over short distances, demonstrating that their complexity over tens of kilometers along depositional strike is much greater than previous studies have suggested.

### Study Area

The Green River Fm. cropping out in the east-to-west trending Nine Mile Canyon is the focus of this and many previous studies (Jacob 1969; Ryder et al. 1976; Remy 1991; Keighley et al. 2002; Pusca 2004; Taylor

and Ritts 2004; Schomacker et al. 2010; Moore et al. 2012; Gall et al. 2017; Birgenheier et al. 2020; Wang and Plink-Björklund 2020) along the border of Duchesne and Carbon counties, roughly 60 km NE of Price, Utah (Fig. 2). The Nine Mile Canyon area is ideal for large-scale outcrop correlation and investigation inasmuch as there is minimal E to W dip ( $\sim 1^\circ$ ) and consistent exposure of the Sunnyside Interval of the Green River Fm. The main canyon has numerous side canyons (Argyle, Gate, Daddy, and Cottonwood canyons) that provide perpendicular N to S exposures (Fig. 2). This three-dimensional outcrop coverage is important for regional or sub-regional correlations and for understanding the variability of sedimentary architectures. Exposures of Sunnyside Interval diminish eastward due to many of the lower markers dipping below the canyon floor (Spinnangr 2014).

### GEOLOGIC BACKGROUND

#### Laramide Intermontane Basins

The Paleogene Uinta Basin is a ponded intermontane basin (Dickinson et al. 1988) in the Laramide structural province. It was formed in the Late Cretaceous to early Cenozoic as a result of basement shortening due to flat slab subduction and the partitioning of the once-extensive Cretaceous Sevier (Cordilleran) foreland basin, which represents a fundamental shift in the geologic history of the western USA (Dickinson and Snyder 1978). The Uinta basin is classified as *ponded* due to the existence of long-lived

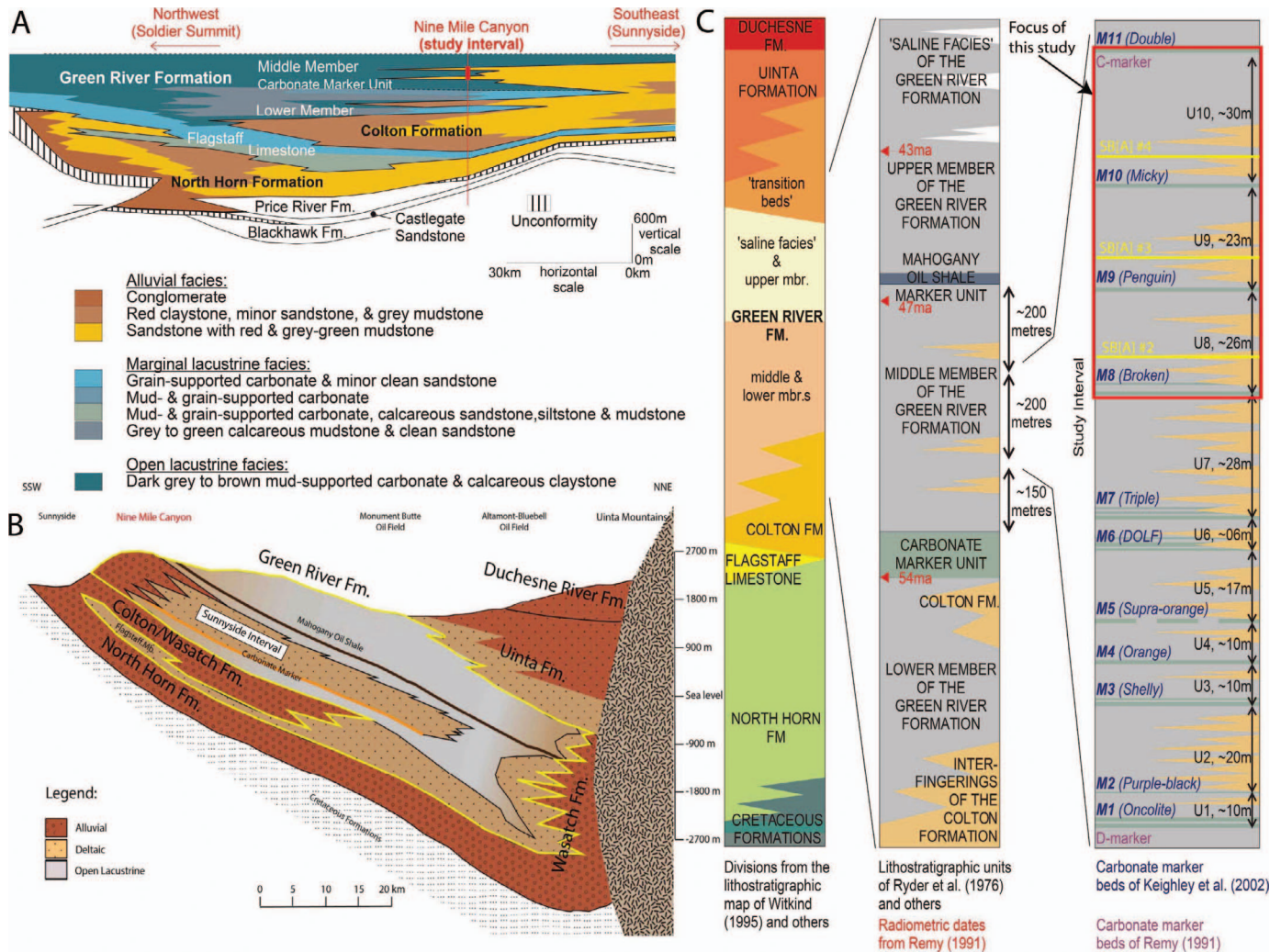


FIG. 3.—**A**) Oblique transect of the Uinta Basin (from Keighley et al. 2002 after Ryder et al. 1976). **B**) N–S transect of the Uinta Basin (from Spinnangr 2014 after Keighley et al. 2003). **C**) Stratigraphy of the Uinta Basin and the Sunnyside Interval with carbonate markers and sequence boundaries from Keighley et al. (2003).

lacustrine environments with adjacent structural barriers that promoted an endorheic setting and which served as the final sink for a large part of the southern Sevier foreland basin drainage system (Dickinson and Snyder 1978; Lawton 2019). It is one of the largest ponded Laramide basins (ca. 200 km E–W and 150 km N–S) and is bounded to the north by the Uinta Mountains, to the southeast by the Uncompahgre uplift, and to the southwest by the San Rafael Swell (Lawton 2019). The basin was connected occasionally to the eastern Piceance Basin, though not during the stratigraphic interval of this study (Johnson 1985).

#### Uinta Basin Stratigraphy

The appearance of lacustrine facies in the Green River Formation marks the onset of the long-lived, internally draining lake system (Fig. 3). The study area, Nine Mile Canyon in Utah, is hosted on the southern limb of a syncline with regional dips of < 5° north and ~ 1° east. The original southern basin margin may have been up to 50 km south of the study area (Keighley et al. 2003). The earliest continental basin sediments comprise the North Horn Formation (Maastrichtian to late Paleocene) (Johnson 1985), a large fluvio-deltaic complex sourced from the Sevier thrust front and which flowed eastward depositing red mudstones, alluvial sandstones,

and lacustrine siltstones and claystones (Johnson 1985). To the south, the San Rafael Swell impounded east-flowing drainages out of the Flagstaff Basin, leading to extensive carbonate precipitation—the first signal of the presence of a widespread lake forming the Flagstaff Member of the Green River Formation (Stanley and Collinson 1979). The Flagstaff Member grades up into the Carbonate Marker Unit (CMU), an ~ 30-m-thick unit of ooid-and-ostracod bearing marginal carbonate facies with basin-center organic-rich mudstone and kerogenous oil shale (Ryder et al. 1976; Remy 1991). A renewal of siliciclastic input led to the fluvio-lacustrine “Sunnyside Delta Interval” (hereafter referred to as the Sunnyside Interval in order to remove interpretive naming) of Remy (1991) (Fig. 3). The CMU, the Sunnyside Interval, and the overlying Transitional Interval is contained in the middle Member of the Green River Formation. The focus of this study is the ~ 200-m-thick upper half of the Sunnyside Interval (Fig. 3).

#### Sunnyside Interval Stratigraphy: Previous Interpretations

Remy (1991) provided a high-resolution correlation of the Sunnyside Interval using laterally continuous carbonate markers which generally followed the D (oldest) to A (youngest) marker beds of Jacob (1969). The

lower half of the Sunnyside Interval is mainly lacustrine carbonates of variable grain size and composition capped by the D marker of Jacob (1969) at about 160 m above the CMU (Spinnangr 2014). The upper half of the Sunnyside Interval consists of cyclic fluvial units interbedded with grain-dominated lacustrine carbonates, calcareous siltstones, and mudstones (Fig. 3). The carbonate markers (D marker to C2 marker) utilized by Keighley et al. (2002) are used in this study as marker horizons (Fig. 3). Between the D and C2 markers there are nine additional discrete carbonate marker horizons that further subdivide the Sunnyside Interval into ten cyclic packages (Fig. 3). These markers were named M1 to M11 by Keighley et al. (2002), where M1 is equivalent to the D marker of Jacob (1969) and Remy (1991) and M11 is equivalent to the C2 marker from those studies. The ten intervening intervals are typically composed of ~ 20-m-thick floodplain deposits (channel sandstones, fine-grained overbank deposits, crevasse or terminal splays, and pedogenic mudstones) and ~ 10-m-thick lacustrine-dominated intervals (fine-grained tabular mouth bars or delta fronts, grain-supported carbonates, or lacustrine mudstones) (Fig. 3).

#### Lacustrine Sequence Stratigraphy

Sequence stratigraphy, a chronological framework of study for stratal stacking pattern analysis, has been successfully applied in a variety of depositional settings for decades in sedimentary geology (Brown and Fisher 1977; Mitchum and Vail 1977; Johnson and Murphy 1984; Posamentier and Vail 1988; Van Wagoner et al. 1988, 1990; Mitchum and Van Wagoner 1991; Embry and Johannessen 1993; Helland-Hansen and Gjelberg 1994; Neal and Abreu 2009; Catuneanu et al. 2009). Several schools of sequence stratigraphic thought were synthesized into a model-independent framework by Catuneanu et al. (2009) which is adopted within the current work. While this relatively recent generalization of sequence stratigraphy has enabled the methodology to be more widely applicable, the stratal organization of continental closed lacustrine environments remain organizationally enigmatic and inconsistently interpreted at a variety of scales.

Previous workers have attempted to reconcile closed lacustrine sedimentary successions with sequence stratigraphic concepts (Shanley and McCabe 1994; Milligan and Chan 1998; Lemons and Chan 1999; Bohacs et al. 2000; Bartov et al. 2002; Keighley et al. 2003; Pusca 2004; Ilgar and Nemec 2005; Zou et al. 2010; Moore et al. 2012; Feng et al. 2013, 2016; Nutz et al. 2017, 2020; Gong et al. 2019; Zhang et al. 2020). Shanley and McCabe (1994) argued for interpreting both lacustrine and shallow marine strata in the sequence-stratigraphic framework, but with careful consideration of the local-to-regional climatic shifts more readily than base-level changes in continental settings. Milligan and Chan (1998) argued that the “Gilbert Deltas” of Pleistocene Lake Bonneville were mostly transgressive in nature and that identified correlative sequence boundaries separate hiatal periods of pedogenic development from periods of higher clastic supply. Bohacs et al. (2000, 2003) made numerous salient observations about the nature of lake sedimentation, noting that closed lacustrine systems host erosionally bounded, thick transgressive deposits but thin to nondepositional lowstand deposits (or lack thereof). Due to the coupled nature of water and sediment routing in closed basins via catchment tributaries, erosive power and sediment carrying capacity increases during lake-level rise and decreases during lake-level fall, explicitly violating the assumptions of Posamentier and Vail (1988) and Bohacs et al. (2000) valid for marine sequences. Bartov et al. (2002) applied sequence stratigraphic methods to Holocene deposits in the Dead Sea, assigning sequence boundaries at the base of clastic-rich marginal sedimentary pulses with well-constrained radiocarbon dates. Keighley et al. (2003) proposed a novel sequence stratigraphic framework for the Sunnyside Interval, modifying the proposed model of Van Wagoner et al. (1988) by identifying sequence boundaries not only by erosional

unconformities (Type A sequence boundaries) but considering lateral facies successions reflective of overall progradation (Type B sequence boundaries). Pusca (2004) recognized a bipartite nature of the Sunnyside Interval depositional sequences, splitting sequences into dry and wet hemicycles which are characteristically transgressive through time. Ilgar and Nemec (2005) applied sequence stratigraphy to early Miocene lacustrine deposits in Ermenek Basin, Turkey, finding that sequences reflect the increased supply and lakeward transport of sediment during lake-level rise and have considerable intra-sequence lateral variability. Moore et al. (2012) revisited the Sunnyside Interval and argued that the cyclic packages of strata should be interpreted as lacustrine parasequences subdivided by flooding surfaces. Feng et al. (2013, 2016) interpreted several long-lived, structurally bounded Eocene lacustrine deposits in China as tectonically driven sequences on first-order to third-order scales. Gong et al. (2019) compared 27 marine and 23 lacustrine clinothem pairs and found distinct differences between sediment delivery and partitioning between marine and lacustrine systems, strongly warning against applying conventional marine sequence stratigraphy to lacustrine basins. Nutz et al. (2017, 2020) applied sequence stratigraphy to paleo-Lake Turkana in the East African Rift system, finding that rift-shoulder-controlled sediment supply had a distinct effect on the resultant lake-margin stratigraphy and that high-and-low frequency sequences (millions to tens of thousands of years) likely have a large orbital forcing component. Nutz et al. (2017, 2020) also found that deep, closed rift lakes can be well interpreted with conventional sequence stratigraphic principles (i.e., progradational lowstand deposits), indicating a volume threshold past which lakes may better approximate marine basins. Zhang et al. (2020) used a mass-balance approach to model lacustrine clinoforms in a closed basin, finding that existing sequence stratigraphic models cannot be directly applied to closed lacustrine systems. These works, despite differences in depositional and tectonic settings along with varying interpretive techniques and experimental design, all provide consistent warnings about applying sequence stratigraphy to lacustrine basins:

Lake base level oscillates at much higher frequencies than eustatic sea level and exhibits more inherent variability (Huybers et al. 2016). This is caused by a myriad of climatic, tectonic, and physiographic influences. In fact, the natural variations in precipitation and evaporation expected under a constant climate can cause decadal to centennial variations in closed-lake base levels. These base-level variations approximate white noise, demonstrating that the random variability in the climate system can cause large and sustained fluctuations in closed-lake water levels that have no direct alloogenetic forcing.

Closed lakes are much more sensitive to changes in sediment supply than marine basins. In closed basins, sediment supply and accommodation creation are directly coupled as water and sediment are routed through the same conduits (tributary rivers). This is not the case in marine settings, where glacio-eustasy, aquifer eustasy, and even steric effects exert fundamental controls on accommodation (sea-level) creation but not sediment supply. There may be an upper limit to this sensitivity depending on the volume or hypsometry of the lake, whereby deep, closed lakes (such as those in the African Rift Valley) are large enough to effectively “unlink” the relationship between accommodation creation and sediment supply and therefore operate stratigraphically more like ocean basins (Nutz et al. 2017, 2020). Due to the coupled nature of base level and sedimentation in closed lakes, lake-level rise is associated with volumetrically large, clastic-rich transgressive deposits. Lake-level drawdown leaves little stratigraphic (depositional) signal but rather exposes underlying strata. Stratigraphic boundaries marking the onset of regional sedimentation are more readily correlative than signals of base-level change in lacustrine systems.

The aim of this study is to synthesize these observations, techniques, and conclusions into a unified sequence stratigraphic framework for closed lacustrine basins and apply it to the Sunnyside Interval.

TABLE 1.—*Facies from Nine Mile Canyon, UT.*

Code	Dominant Sedimentary Structures	Grain Size/Lithology	Interpretation
F1	Conglomerate non-graded-inverse graded-normal graded	Pebble to granule clasts, sometimes micrite. Bed thickness: cm to dm scale (Fig. 4B). Typical erosional and subordinate sharp basal contacts. Upper contacts are generally sharp. Clasts are commonly planar stratified with subordinate imbrication. Rare inverse grading. Bioturbation is rare. Clasts are one of three compositions: 1) ovoid, subrounded to well rounded gravel to pebble-sized clasts; 2) angular micrite clasts, gravel to pebble size; 3) bioclastics: shells, ooids, ostracods, rare fish scales, and vertebrate bone fragments.	Turbulent subaqueous sediment gravity flows at base of massive, deformed, or planar-laminated sandstones. Flows likely generated by river floods, sometimes incorporating exposed carbonate or weathered clasts on the exposed lake plain, possibly desert pavement in origin.
F2	Plane-parallel lamination	Fine- to medium-grained sandstone, bedding contacts are generally sharp but non-erosional (Fig. 4E). Occasional vertical burrows. Typical bed thickness: dm to m scale. Laminae are typically cm-scale. This facies forms large portions of cliff-forming sandstones, with deformed (F8) to conglomeratic (F1) facies below and rippled facies (F5) above.	Unidirectional current with upper-flow-regime conditions (Berg and Gelder 1993) suggesting subaerial to shallow-water constrained flows proximal to river-mouth area.
F3	Trough cross-stratification	Fine- to medium-grained cross-stratified sandstone. Occasionally varnished. Bedding contacts are generally gradational. Cross-sets are 3–7 cm. Facies appears usually in the middle third of m-scale sand bodies. Facies F3 is not very common.	Unidirectional current deposition in the upper portion of the lower flow regime (Berg and Gelder 1993). Representing 3-D-crested small subaqueous dunes.
F4	Planar tabular cross-stratification	Fine- to medium-grained cross-stratified sandstone. Occurs inside massive cliff-forming sandstones, typically near the bottom of the unit but above the basal lag deposits of F1, cross laminae are occasionally deformed. Bedding contacts are typically sharp and cross-set size is larger than F3, ranging from ~5 cm to 15 cm. Bioturbation is rare (Fig. 4F). Facies F4 is not common.	Cross bedding indicates middle lower-flow-regime conditions of unidirectional currents, forming subaqueous dunes inside channels. Tabular cross-bedding is relatively rare compared to trough cross-bedding.
F5	Asymmetric-ripple cross stratification	Fine-to-very fine-grained ripple cross-stratification sandstone (Fig. 4A). It is a common facies, occurring in either A) large, meter-scale, cliff-forming sandstones or B) thin, tabular, calcareous and lenticular (slightly channelized) to laterally continuous (at outcrop scale) beds. Bioturbation is common in F5B facies, especially near tops of beds. Bioturbation is rare in the F5A facies. F5A commonly occurs above planar-laminated or deformed sandstones, with siltstones overlying them. F5B facies are typically surrounded by siltstones, mudstones (both red and gray), or more rarely, shallow-water carbonates (F14 and F16).	Unidirectional flow ripples in lower portion of lower flow regime (Berg and Gelder 1993). When inside m-scale cliff-forming sandstones (F5A), depositional environment is likely subaerial to littoral channel deposition, indicating the waning stage of ephemeral floods. F5B likely indicates either 1) crevasse splay or lake plain flood events (when surrounded by oxidized mudstone (F12), or 2) subaqueous deposition on the delta front (subaqueous lobes).
F6	Climbing-ripple cross-lamination	Fine- to very fine-grained ripple cross-laminated sandstone. F6 facies occur in dm-scale beds surrounded by siltstones or mudstones (red and gray). Ripple heights range from 3 to 7 cm. The cross-sets have a climbing trajectory.	Subaqueous unidirectional flow with high sediment flux under waxing flow conditions (McKee 1965). Likely deposited in a flow expansion area such as the mouth of a crevasse splay or distributary channels.
F7	Scour-and-fill sandstone	Medium- to fine-grained sandstone, common in meters-thick cliff-forming sandstones	Turbulent, variable-velocity flows with high velocity triggering local erosion. The scours might be part of large supercritical bedforms such as cyclic steps? (Wang and Plink-Björklund 2020)
F8	Deformed sandstone	Fine- to medium-grained sandstone with deformed sedimentary structures. The beds are often erosional and contain woody fragments at the base (Fig. 4G). Mostly in m-thick sandstones, typically appearing in the bottom third of the unit. Deformed strata range from cm-scale to multi-meter scale, indicating a range in magnitude of overburden stress. Deformed strata are typically planar laminated or more rarely large-scale cross-stratified.	Rapid deposition and post depositional soft-sediment deformation. This facies may represent saturated loading and subsequent liquefaction of strata from overlying sandstone (Töro et al. 2015), maybe stemming from the flashy discharge posited by Wang et al. (2019).
F9	Green mudstone, structureless, bioturbated	Clay- to silt-dominated mudstone, often nodular and calcareous. Calcite and/or gypsum veins are common (Fig. 6C) Bed thickness: cm-scale to half-meter scale. Occasionally rooted and bioturbated (vertical burrows). The green color of this facies may be largely diagenetic, indicated by its relationship to overlying sandstone bodies and red mudstone. Often deformed by overlying sandstone.	Lake inundated siltstones and mudstones deposited in the medial to distal prodelta or off-axis. Alternatively, floodplain or exposed floodplain that underwent subsequent reducing diagenesis.

TABLE 1.—Continued.

Code	Dominant Sedimentary Structures	Grain Size/Lithology	Interpretation
F10	Red mudstone, laminated, bioturbated	Mud to silt dominated mudstone, occasionally mottled, commonly rooted and occasional desiccation cracks (Fig. 5). Sometimes nodular and calcareous. This facies is occasionally laminated, though bioturbation may obscure much of original bedding structure. Sometimes deformed by overlying sandstone beds.	Exposed floodplain that was seasonally or temporarily flooded. The red color is a product of the oxidation of iron-bearing minerals, possibly hematite (Remy 1991).
F11	Gray mudstone, laminated	Clay to very fine silty mudstone, laminated, occasionally bioturbated (Fig. 6A). Occasionally deformed by overlying sandstone beds. F11 is a rarely occurring facies.	Deeper (beyond fair-weather wave depth) lacustrine deposition from fallout or weak currents. The difference between this facies and F11 is slight, but functionally important. The green color (from ~5% chlorite (Remy 1991)) indicates a shallower environment than darker gray mudstones.
F12	Carbonate Grainstone	Ostracods, ooids, and shells. Ooid grain sizes range from sub-millimeter to millimeter scale (Fig. 5G). Ostracods are 1 to 2 mm. Shell fragments range in size from sub-millimeter to 10 cm. Bed thickness ranges from decimeter scale to more commonly 50 to 100 cm. Ostracod beds typically cap limestone or sandstone beds and are commonly orange stained. Grainstones rarely show sedimentary structures like cross-bedding or planar lamination.	Littoral deposition under little to no clastic input, possibly in the swash zone under weak wave currents. Poorly sorted bioclastic grainstones may be storm deposits. Orange staining is interpreted as oxidized iron-bearing minerals as a result of subaerial exposure.
F13	Undifferentiated sandstone–marlstone–siltstone	Silt to fine-grained sandstone, typically calcareous (fizzes with HCl), occasionally rippled; bed thicknesses range from dm to half-m scale, but never larger. Beds occur either isolated, surrounded by siltstone and mudstone, or in bedsets below overlying sandstone. Bed boundaries are typically sharp, often interbedded with siltstone. Obvious bioturbation signals are uncommon, though it may be so extensive that the beds appear structureless (Fig. 6).	Tabular mouth bar and delta front deposition—off distributary channel axis? Possible lake-plain crevasse deposition which was subsequently inundated and diagenetically altered.
F14	Stromatolite–thrombolite	Laminated to rarely clotted carbonates. Dominant fabrics are agglutinated or fine grained. Beds are domal to planar to chaotic. Beds are generally orange stained with a wide range of grain sizes: from mud to medium-size sand grains. Thicknesses range from 0.1 to 0.5 meter (Fig. 7).	Laminated benthic microbial deposits after Riding (2011) which form in the sublittoral zone from active microbial growth and incorporation of clastic grains. Previous workers have identified these bedforms representing a sublittoral to lower-littoral environment in the eastern Piceance Basin, Colorado (Eljalaf 2017).
F15	Oil shale	Kerogenous claystone, bright purple-black organic-rich, TOC% up to 15% (Ruble et al. 2001), mm-scale laminae (Fig. 7D)	Shallow-dry lake setting where turbid, eutrophic pools exist on the surface with a shallow photic zone, preserving organic material.
F16	Micrite	Carbonate mud to quartzose wackestone typically surrounded by F14, F15, F16, or F17. Bed thicknesses: dm to m scale. Contacts are sharp but have occasional intra-bed gradational contacts with grainstones or siltstones. Weathered surface is generally orange to yellow, fresh surface is dark-gray to yellow. Sedimentary structures are vanishingly rare.	Sublittoral precipitation of authigenic carbonates which trap errant sediment grains through baffling or binding (Eljalaf 2017). This occurs at shallower water depths than F14.

## METHODS

### Measured Section

A total of 22 measured sections from published and unpublished sources were correlated across Nine Mile Canyon (Fig. 2), including seven new measured sections targeting cycles between the M8 and M11 markers of Keighley et al. (2003). All together, these sections total ~600 m of high-resolution stratigraphic data. Measured sections record bed lithology, thickness, physical and biological structures, bioturbation intensity, upper and lower bedding contacts, and paleocurrent orientations.

To aid in stratigraphic correlation of the measured sections, a commercially available unmanned aerial vehicle, the DJI Mavic Pro II, was flown throughout large parts of Nine Mile Canyon in order to construct orthophotomosaics. The software Agisoft Pro Metashape was used to construct 3-D tiled drone models. On the correlation panel, measured sections are positioned laterally in accurate proportion to their

real-world locations. Sequences and bed correlations were constructed by on-site surveying and later aided by aerial-photo-generated orthophoto-mosaics. Facies and facies associations were generated during field measurements of logs and creation of cross sections as outlined below.

### Facies and Facies Associations

Observed deposits were separated into 16 distinct facies (Table 1) based on their sedimentological characteristics such as lithology, physical and biological sedimentary structures, and bedding contacts (Table 1). Facies lithologies are highly variable in every sequence, ranging from mudstone to pebbly medium-grained sandstone for siliciclastic deposits and grainstones to micrites and stromatolites for carbonate deposits (Table 1). Five facies associations (FAs) were developed based on depositional environments:

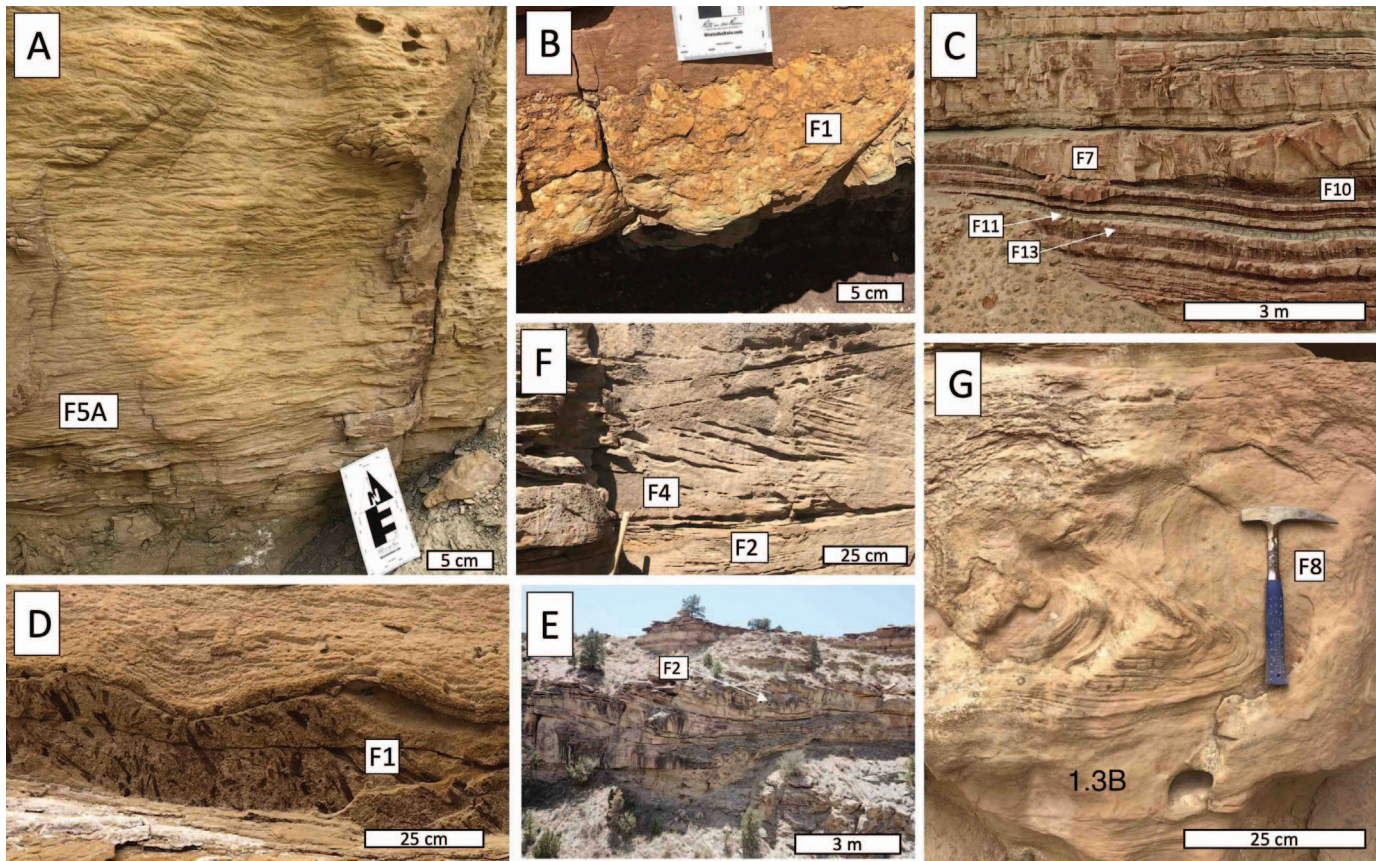


FIG. 4.—Facies Association 1: channelized subaerially deposited sandstones. **A**) Thick, rippled sandstone channel deposit. **B**) Micrite-rich basal-lag conglomerate common to the base of thick FA1 channel deposits. **C**) FA1 thin channelized sandstone deposit scouring into underlying FA2 floodplain deposits near Blind Canyon. **D**) Woody debris at the base of an FA1 deposit. **E**) Large FA1 deposit showing in-channel bar architecture in Gate Canyon. **F**) Planar cross-bedding inside FA1 deposits. **G**) Common intra-unit soft-sediment deformation and slumping near the entrance of Nine Mile Canyon.

**FA1 Channelized Subaerially Deposited Sandstones.**—FA1 deposits consist of amalgamated upper-medium to more commonly fine-grained, quartz-rich sandstones with common 10-cm-scale basal lag conglomerates (F1; Fig. 4B). Bed thickness ranges from decimeter-scale to multiple meters of amalgamated sandstone beds. FA1 is generally laterally continuous. Channel infill facies are notably aggradational, exhibiting genetically linked flow-waning successions throughout infilling units (Fig. 4: F1, F2, F7, F8, F3, F4, F5A). The bedding types will be further discussed but consist of four specific geometries: thin and tabular, shingled, channelized and lenticular, and tabular and amalgamated.

**FA2 Subaerially Exposed Lake Plain.**—FA2 deposits are red (F10) and occasionally gray-green (Fig. 5A; facies F9, F11) mudstones or mud-rich siltstones with rootlets, pedogenic characteristics (e.g., rhizoliths), and occasional desiccation cracks (Fig. 5B). Centimeter-scale planar lamination of variable grain sizes (mud to very fine sand) is typical (Fig. 5A). Lenticular, thin sandstone stringers (5–15 cm) are common (F13), exhibiting planar lamination (F2) or ripples (F5A) (Fig. 4A). Sandstone beds are identified as terminal or crevasse splays depending on their thickness and lateral continuity.

**FA3 Littoral to Sublittoral Clastics.**—FA3 deposits are thin (cm-dm), tabular sandstone and siltstone beds (Fig. 6D, E; facies F13) with unidirectional-current structures (F5B) or planar lamination. FA3 deposits are typically a variable mix of silt, very fine sand, and authigenic carbonates. FA3 occurs in two forms: bedsets (10–20 beds) of laterally

continuous dm-scale very fine sandstone to siltstone (Fig. 6D, E; facies F13), and isolated tabular beds (decimeter-scale) surrounded by sublacustrine mudstones and fine siltstones (Fig. 6A, C; facies F9, F11). These beds have a high calcareous content (react readily with HCl).

**FA4 Littoral to Sublittoral Carbonates.**—FA4 deposits consist of high- to low-energy- environment carbonate deposits. Littoral deposits are generally: 1) ooid and ostracod grainstones with subordinate shell fragments (Fig. 7G; facies F12); 2) micrites (Fig. 7G; facies F16) in the form of dm- to m-scale thick carbonate mudstones to quartzose wackestones typically surrounded by facies F14, F15, F16, or F17 (Fig. 7A, D, G). Micrite deposits have occasional intra-bed gradational contacts with grainstones or siltstones (Fig. 7G); 3) sublittoral stromatolites and rare thrombolites (F14) which occur at the top of carbonate beds (Fig. 7A–C, E). Sublittoral carbonates are more common in the southern and eastern sections of the field site. FA4 is almost always orange-stained (indicating subaerial exposure, e.g., Fig. 7) and may occasionally exhibit bioclastic cohesive flows of remobilized carbonate grains (F1).

**FA5 Anoxic Strata.**—FA5 deposits are the rarest in the study sections measured and consist of organic-rich, dolomitic kerogenous oil shales (Fig. 7D; facies F15; Remy 1991). FA5 is a rare facies association that is laterally discontinuous, occasionally exhibiting fossils. The depositional environment is interpreted as shallow turbid pools of low-energy, anoxic biogenesis below the photic-zone. In lakes, photic-zone depth varies. In highly turbid and eutrophic lakes the photic zone can be as shallow as 50

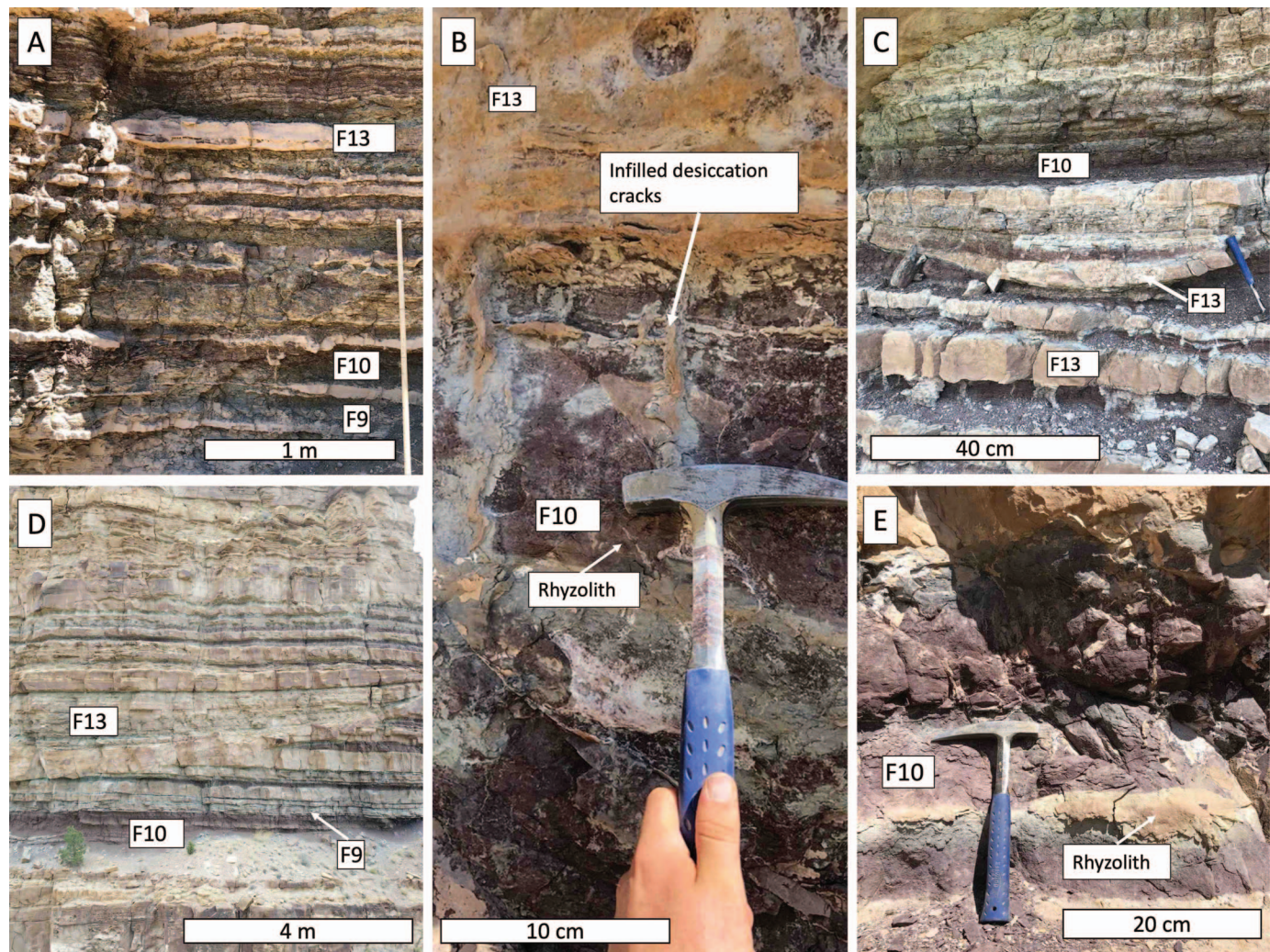


FIG. 5.—Facies Association 2: well-drained floodplain deposits. **A)** Common floodplain succession showing pedogenic mudstone and siltstone as well as marly to sand-rich “stringers” or thin, tabular beds. **B)** FA2 deposit overlain by an FA4 carbonate grainstone. Both surfaces show evidence of exposure; the FA4 carbonate is orange-stained and infilling desiccation cracks of the FA4 pedogenic mudstone. Rhizoliths are also common in FA2 deposits. **C)** Common FA2 sequence showing a sandstone floodplain channel filled with upward-deepening facies patterns including both subaerially exposed and subaqueous mudstone and siltstone. **D)** FA1 channel downcutting into FA2 deposits. The FA1 channel is filled with subaqueously deposited strata, indicating a transgression. **E)** Pedogenic red mudstone with rhizoliths and overlain by FA4 exposed carbonate grainstone deposits.

cm (Hecky and Kilham 1973; Koenings and Edmundson 1991; Jackson 2003). Additionally, shallow saline lakes can host high-TOC (> 6%) surficial sediments including oil shales (Boon 1983; Burne and Ferguson 1983).

Annotated facies associations for parts of logs G2 and G6 (Fig. 8) demonstrate the large amounts of vertical FA variability, suggesting drastically different depositional environments within only several meters of section.

#### Sandstone Bedding Geometries

Within the channelized sandstone facies association, FA1, four bedding geometries are described. Tabular bedding (Fig. 9A) has sharp-based beds which range from decimeter- to meter-scale thick sandstone bodies, commonly interbedded with siltstones and lateral to shingled bedding and erosional based or tabular amalgamated beds. Shingled bedding (Fig. 9C) has sharply bedded, sigmoidal to planar to rare curvilinear sandstone bodies when viewed in outcrop. Bed thickness ranges from decimeter- to

meter-scale beds, sometimes within the same unit. Shingled bedding styles do not have a preferred orientation of the accretion surfaces, generally dipping and thinning or grading laterally into erosional based sandstone bodies or tabular amalgamated beds. Beds can be heterolithic but are generally sandstone-rich and amalgamated (Fig. 9B). Channelized (Fig. 9D) bedding styles are erosional, lenticular sandstones with at least one identifiable channel margin (indicated by a concave shape of sandstone bed). Beds are sometimes concave up but occasionally exhibit inclined or even sigmoidal geometries, which may be a result of outcrop exposure rather than original depositional geometries. Channel beds often change into shingled bedding laterally. Tabular amalgamated units (Fig. 9B) have erosional and non-erosional sandstone bodies which display several amalgamated beds. This bedding geometry is the thickest (2–8 m) and typically changes laterally into shingled beds or, more rarely, channelized sandstone bodies.

The four bedding-geometry types are displayed on the cross-section correlations (Fig. 10). This process was iterative, involving double-checking measured section with collocated orthophotomosaics.

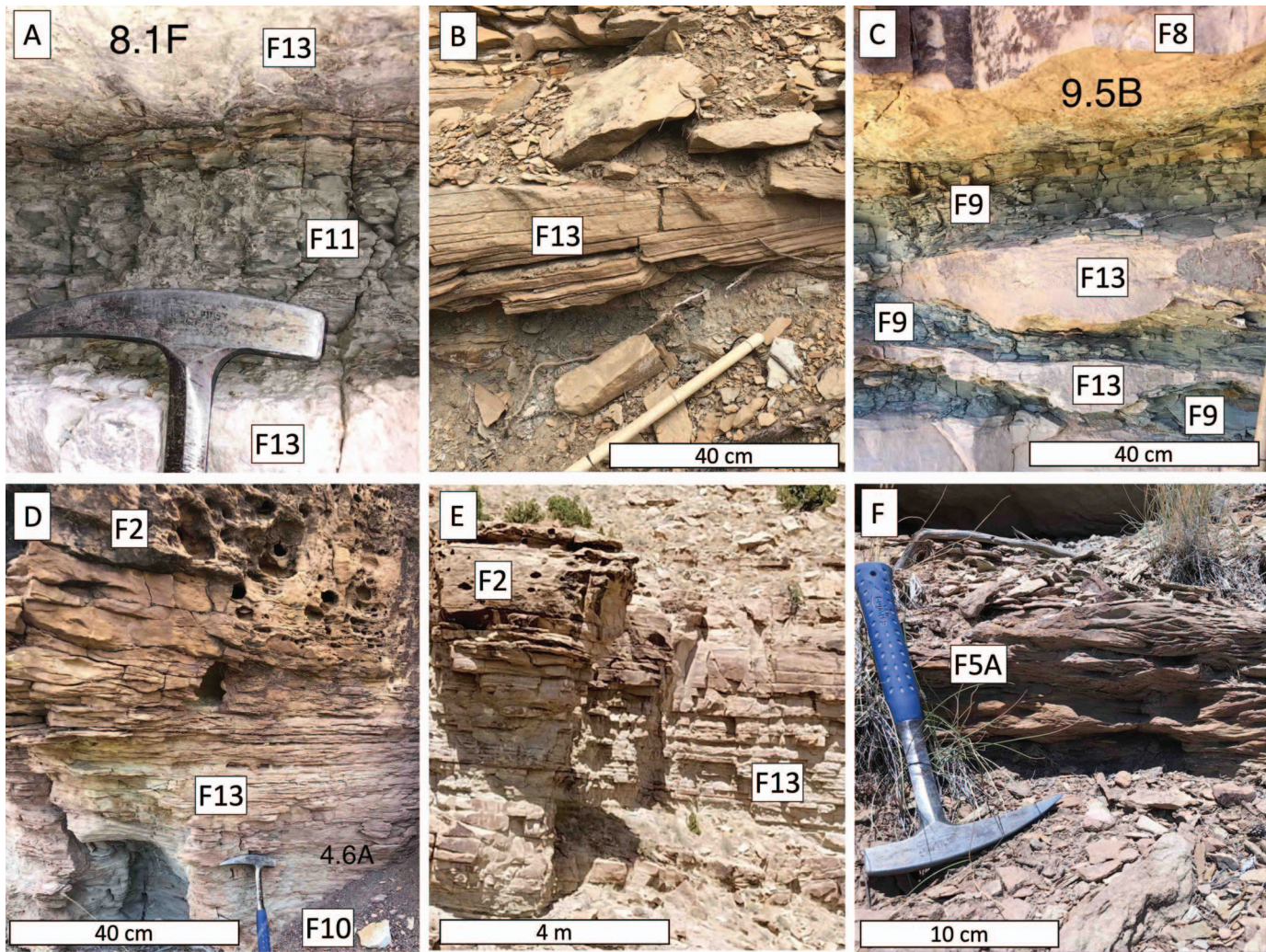


FIG. 6.—Facies Association 3: littoral to sublittoral clastics. **A)** Subaqueously deposited siltstone that has been altered by diagenesis, making it slightly calcite rich. The deposits are between F13 undifferentiated siltstones to marlstones. **B)** Thickening-upward very fine sandstone deposits indicative of a subaqueous progradational setting. **C)** Subaqueous erosional sandstone lenses interbedded with calcite- or dolomite-rich siltstone. These deposits are deformed by a thick, overlying FA1 deposit. **D)** Progradational section of calcite- or dolomite-rich very fine sandstone becoming more sand-rich upsection. **E)** FA3 units conformably overlain by FA1 channelized sandstone deposit. The FA3 units are generally laterally extensive and always calcareous. **F)** Thinly bedded, rippled FA3 deposit interbedded with subaqueous siltstone deposits.

#### Correlation

In total, the 22 measured sections were collated (Fig. 10) to construct the largest known outcrop-based correlation panel to date of the Sunnyside Interval in Nine Mile Canyon. The five data sources are: Remy (1991), Keighley et al. (2002), Pusca (2004), Spinnangr (2014), and Gearon (this study). The correlation panel spans  $\sim$  30 km from W to E. Logs were scaled to the same vertical reference frame using Adobe Illustrator. The sequences and markers of Keighley et al. (2002) were noted on the logs from that study and then traced through the other measured sections, assisting in regional alignment of data. The cross section was flattened on the easily identifiable M9 marker of Keighley et al. (2002), and three previously defined sequences were selected for analysis and reclassification in detail (Fig. 3). These sequences are the SB[A] #2, #3, and #4 of Keighley et al., (2002) that correlate to the units between M8 and M11 (Fig. 3). These upper stratigraphic sequences of Keighley et al. (2003) were chosen for re-examination based on 1) the data availability of the measured sections, 2) the occurrence of laterally extensive, cliff-forming sandstones, 3) the laterally continuous stratigraphy of carbonate markers within the

younger (higher) sequences compared to the lithologically variable and stratigraphically complex older (lower) sequences of Keighley et al. (2002) where multiple carbonate markers can occur, and 4) the fact that previous workers have focused on these lower sequences in detail (Ryder et al. 1976; Keighley et al. 2002, 2021; Keighley and Flint 2008; Schomacker et al. 2010; Wang and Plink-Björklund 2020).

#### LATERAL AND VERTICAL VARIABILITY OF FACIES ASSOCIATIONS

The regional W-E correlation panel along Nine Mile Canyon is oriented along depositional strike to slightly oblique relative to regional paleocurrents and progradational trends. The most compelling observation of this new  $\sim$  30 km transect is the lithologic and depositional environmental heterogeneity (Fig. 10) whereby thick, channelized deposits (FA1) can be laterally or vertically adjacent to low-energy facies such as siltstones or mudstones (FA2 and FA3) or even littoral carbonates (FA4), or amalgamated into thick, multi-story channel units (FA1). The most continuous facies associations are subaerial channelized sandstones (FA1) and littoral to sublittoral clastics (FA3), which make up more than 75% of

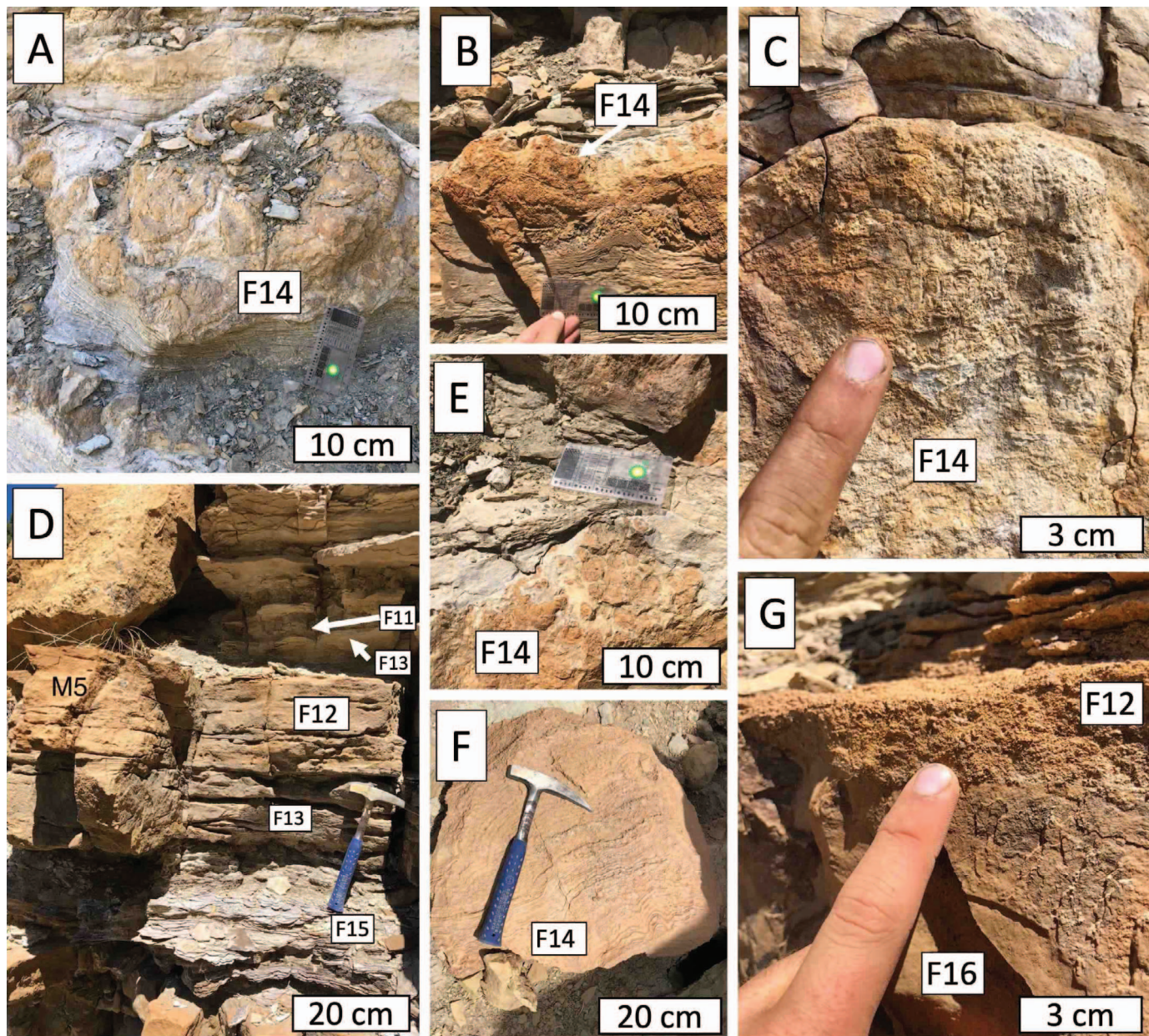


FIG. 7.—Facies Association 4: littoral to sublittoral carbonates. **A)** Large thrombolite showing signs of exposure in Cottonwood Canyon overlying micrite. **B)** Thrombolite in Cottonwood Canyon showing signs of exposure and progression from biolaminites below. **C)** Thrombolite in Cottonwood Canyon displaying clotted fabric and signs of exposure. **D)** Ooid- and ostracod-rich grainstone (M5 marker of Keighley et al. 2003) showing evidence of upward shoaling and exposure. M5 directly overlies an FA5 anoxic strata deposit. **E)** Clotted thrombolite in Cottonwood Canyon. **F)** Well-defined stromatolite found in float near Currant Canyon. **G)** Shoaling-upward carbonate grainstone with large shelly fragments, ostracodes, and ooids.

the annotated cross section (Fig. 10). Throughout the section channelized sandstone deposits (FA1) are almost entirely fine-grained apart from the commonly associated basal lag conglomerates (F1), though they range from very-fine to medium-size grains with no distinct trend from W to E. Observed FA1 facies and sedimentary structures are likewise consistent throughout the section, with only a slight trend from majority trough-cross bedded facies (F3) in the eastern sections to mainly rippled facies (F5) in the western sections of the transect (Fig. 10). FA1 channel-fill styles are largely aggradational, with most thick units containing convolute to deformed bedding (F8) and constructional bedforms (F5, F6). The typical progression of sedimentary structures within FA1 sandstone units is basal scouring with common lag conglomerates (F1) and woody debris followed

by parallel laminae (F2) and scour-and-fill structures (F7). Continuing up-section, a common zone of deformed strata (F8) occurs (Fig. 4G) followed by conformable waning-flow successions of trough cross bedding (F3 and F4) to commonly rippled strata F5A at the top of FA1 sandstone deposits.

Well-drained-floodplain deposits (FA2) are relatively discontinuous, as clearly seen along W-E trends, occurring more commonly in the eastern part of the cross section, which can be interpreted to be slightly proximal given the implied oblique-to-strike orientation of the transect (Fig. 10). Well-drained-floodplain deposits (FA2) can conformably overlie subaqueous strata (FA3, FA4, and FA5) or FA1 channel deposits. These oxidized, rooted, and pedogenic mudstone deposits along with thin (< 50 cm)

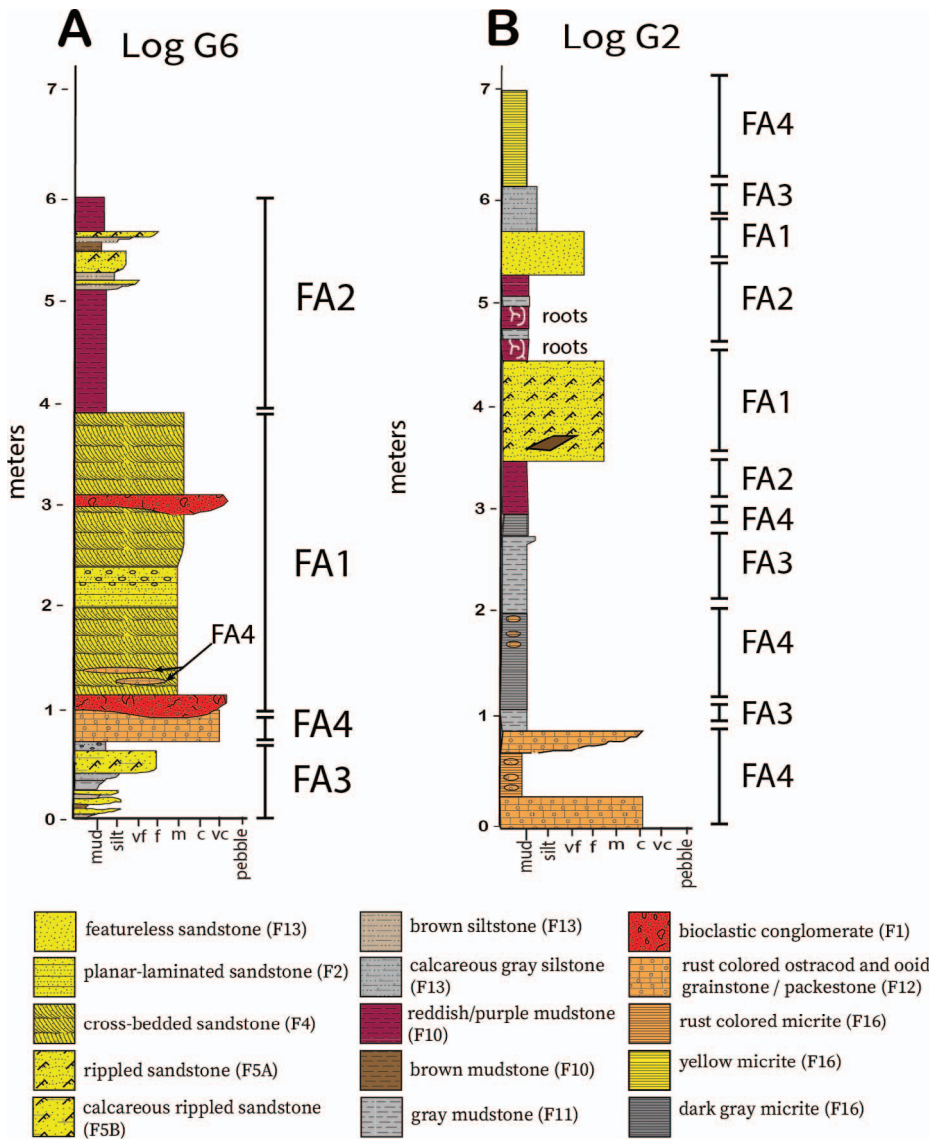


FIG. 8.—Facies Associations for portions of logs G2 and G6 drastically demonstrating changes in depositional environments within several meters of section. **A)** Highlights the disparity in sediment supply above and below the erosional scour into FA4 carbonate below. Additionally, FA1 sandstones often incorporate clasts of FA4 carbonates below. **B)** A less drastic introduction of increased supply to the system, starting as coeval pedogenic floodplain accumulation (FA2) conformably overlying subaqueous mudstones and micrites. Roots are common in FA2 deposits, and woody debris at the base of FA1 deposits indicates the introduction of more energy to the system. Individual facies are included.

sandstone deposits (Fig. 5) are easily identifiable and are far more common in the eastern part of the transect, gradually decreasing westward.

Littoral, sublittoral (FA4), and (rarely) anoxic strata (FA5) conformably overlie the subaqueous clastic deposits of FA3 (Fig. 10A). FA4 deposits are likewise discontinuous but display opposite trends to FA2 deposits, appearing first approximately 1 km from the beginning of the transect in the west (Fig. 10A) and become more abundant up-section. The most discontinuous facies association is FA5, anoxic strata, which is sometimes visible below overlying FA1 sandstones when not scoured away. Due to its rarity, general trends in FA5 emplacement cannot be resolved.

The facies variability along what can be considered approximate chronostratigraphic horizons implies a dynamic near-shoreline environment characterized by differential energies (i.e., inundated floodplain vs. high-energy channelization). The large amounts of high-energy bedforms and basal incisions associated with the channelized deposits (FA1) observed in the Sunnyside Interval is well documented (Jacob 1969; Ryder et al. 1976; Remy 1991; Keighley et al. 2002; Pusca 2004; Taylor and Ritts 2004; Schomacker et al. 2010; Moore et al. 2012; Gall et al. 2017; Birgenheier et al. 2020; Wang and Plink-Björklund 2020).

While the fringes of the Sunnyside Interval system are not recorded in this transect, in the studied interval there are four identifiable axes of

deposition, labeled Axis 1–4 in Figure 10, that persist throughout the correlation panel based on both lateral and vertical facies trends (Fig. 10). Each lobe of deposition is identifiable by consistent lateral emplacement of littoral to sublittoral clastics (FA3) and carbonates (FA4) throughout successive cycles, likely indicating long-lived interdistributary bays (or interfluves during periods of low lake level). Locations of deposition of channelized sandstone (FA1) change through time but stay largely within the identified edges of the axes (Fig. 10). The exception to this can be found in the upper sections of the western part of the correlation panel where thick, channelized sandstone deposits (FA1) occur directly on top of the location of the previous westernmost interdistributary bay (Fig. 10).

#### THE SUPPLY-GENERATED SEQUENCE (SGS)

At its most general definition a stratigraphic “sequence” represents the net product of sedimentation during one complete stratigraphic cycle—a full, cyclic change in accommodation and sediment supply—regardless of whether the complete cycle is formed or preserved (Catuneanu et al. 2009). The bounding surfaces of sequences are “sequence boundaries” which are user-defined but consistently denoted correlative stratal surfaces that can be conformable or unconformable (Catuneanu et al. 2009). Introduced

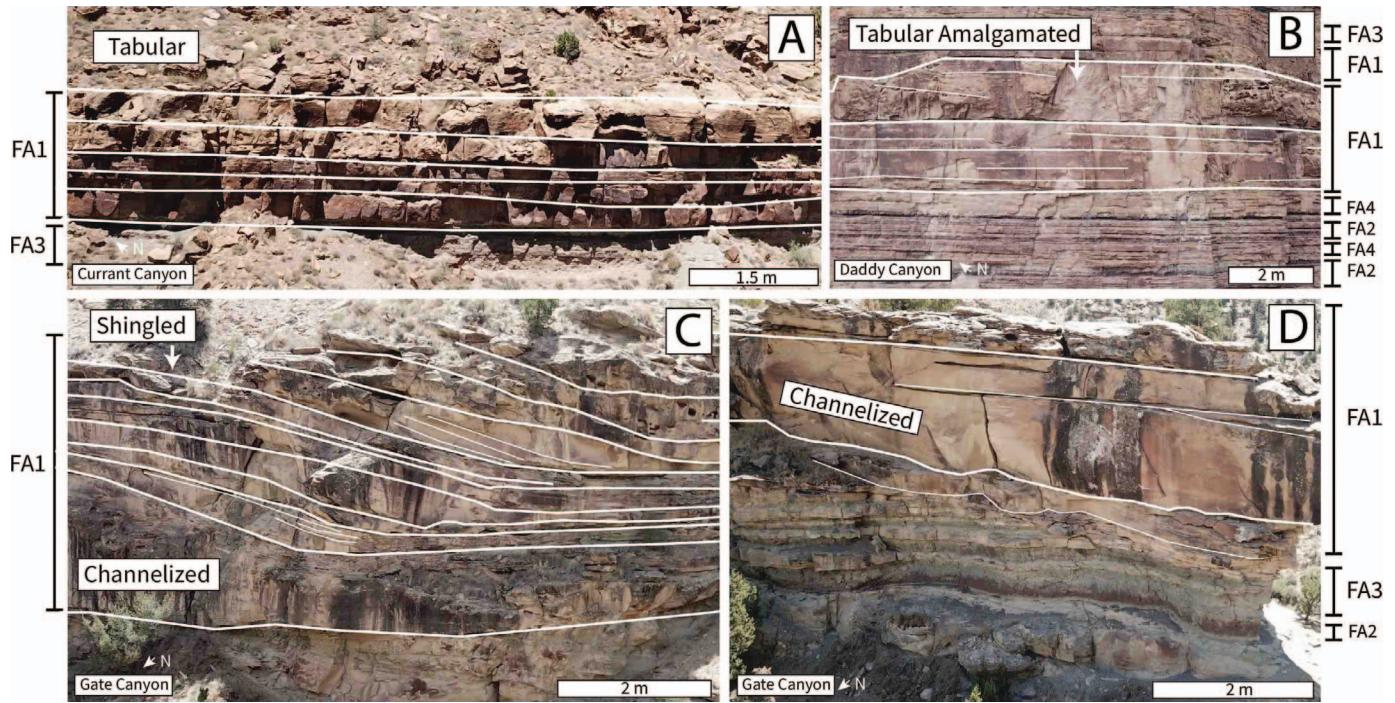


FIG. 9.—FA1 bedding geometries. A range of sandstone bedding geometries were identified to help delineate sequences and connect outcrop logs over large gaps where only drone-based photographic information existed. Tabular bedding geometries are common adjacent to higher-energy bedding geometries like channelized or shingled types. Channelized types are easily identified by large scour surfaces. Tabular amalgamated bedding geometries are most common in the eastern part of the correlation panel and contain numerous internal bedding planes.

here, the supply-generated sequence boundary results from a sub-regional to regional increase in supply of sediment and water identified by correlative surfaces, conformable or unconformable, separating facies or surfaces associated with low clastic supply (e.g., carbonates, mudstones, or desiccation and exposure surfaces) from facies characteristic of relatively higher amounts of clastic supply—in this case, channelized sandstones, subaqueous siltstones and marlstones, aggradational mudstones, and siltstones and sandstones of floodplain deposits. The supply-generated sequences (SGSs), which display predictable geometric and facies successions (Fig. 11) are bounded by sequence boundaries (SGSBs). An SGSB can be erosional, manifesting as an disconformity under the fluvial depositional axes or might occur as a simple vertical facies change representing increased regional sediment influx lateral to fluvial axes such as overbank sedimentation (Fig. 5E), crevasse splays (Fig. 5A), or terminal-splay-style successions (Fig. 5C) (Tunbridge 1981; Stear 1985; Fisher et al. 2008). The SGSB should be placed below the onset of coeval floodplain deposits when no obvious channel deposit is observed (Fig. 11). Additionally, the SGSB should be placed above evidence of widespread exposure such as desiccation features, oxidized carbonate or pedogenic strata, or anoxic strata (FA5). With this methodology, 10 novel SGSBs are identified in the three SB[A] sequences of Keighley et al. (2003) (Fig. 3).

#### **Depositional Architecture of Supply-Generated Sequences Variable-Discharge Origin of FA1 Deposits**

In the Sunnyside Interval, the base of an SGS is best identified by the incision of thick FA1 channelized deposits into underlying subaqueous strata such as littoral, sublittoral, or anoxic carbonates (FA4 and FA5), as defined by Eljalafi (2017), or littoral to sublittoral clastics, (FA3) (Fig. 6). These erosional surfaces, we argue, result from a significant increase in regional siliciclastic sediment supply (as opposed to lake-level fall) based on five lines of logic: 1) The thick, erosionally bounded sandstone deposits

are filled with sedimentary structures indicating upper-flow-regime, transitional, and supercritical bedforms which have been interpreted as rapidly deposited sediment during the waning stages of high-velocity flooding events (see also Wang and Plink-Björklund 2020). 2) Local fluvial unconformities have been interpreted as evidence for out-of-grade rivers returning to equilibrium (Knox 1975). 3) Fluvial profile adjustments, and therefore riverine erosion, inland from coastal zones have been shown to result from changes in climate (Blum 1991), reflected in change of discharge. 4) The depth of erosion for any channel deposit is less than or equal to one channel depth, indicating that the scours are likely not knickpoint generated and therefore not genetically linked to base-level drawdown (Crosby and Whipple 2006; Belmont 2011). 5) In-channel aggradation or the emplacement of vertical accretion sets are commonly reported high-variable discharge signals in both modern and ancient settings (Tunbridge 1981; Stear 1985; Olsen 1989; Zaleha 1997; Kumar 1993; Allen et al. 2013; Gall et al. 2017).

Evidence for the highly dynamic and flashy nature of Sunnyside Interval channels comes from interpretations of supercritical and transitory bedforms as well as aggradational and upstream-accreting bed sets often housed in or around the shingled, channelized, and tabular amalgamated bedding geometries of FA1 (Wang and Plink-Björklund 2020) as formed in variable-discharge rivers. Shingled beds are the most enigmatic bedding style observed in Nine Mile Canyon, displaying a slight W-dipping preference but can commonly appear in opposite dipping bedsets. Shingled beds have been described previously as fluvial in origin, representing point-bar accretion (Jacob 1969; Ryder et al. 1976; Remy 1991; Keighley et al. 2002, 2003; Morgan et al. 2002). Pusca (2004) argued for a terminal fan model where shingled beds are evidence of intermittent, high-discharge flooding pulses building aggradational channel deposits. Recently, they have been reinterpreted as sharp-based mouth-bar deposits (Schomacker et al. 2010) while other workers have furthered the argument for largely fluvial deposition in the form of fast, braided, high-discharge fluvial

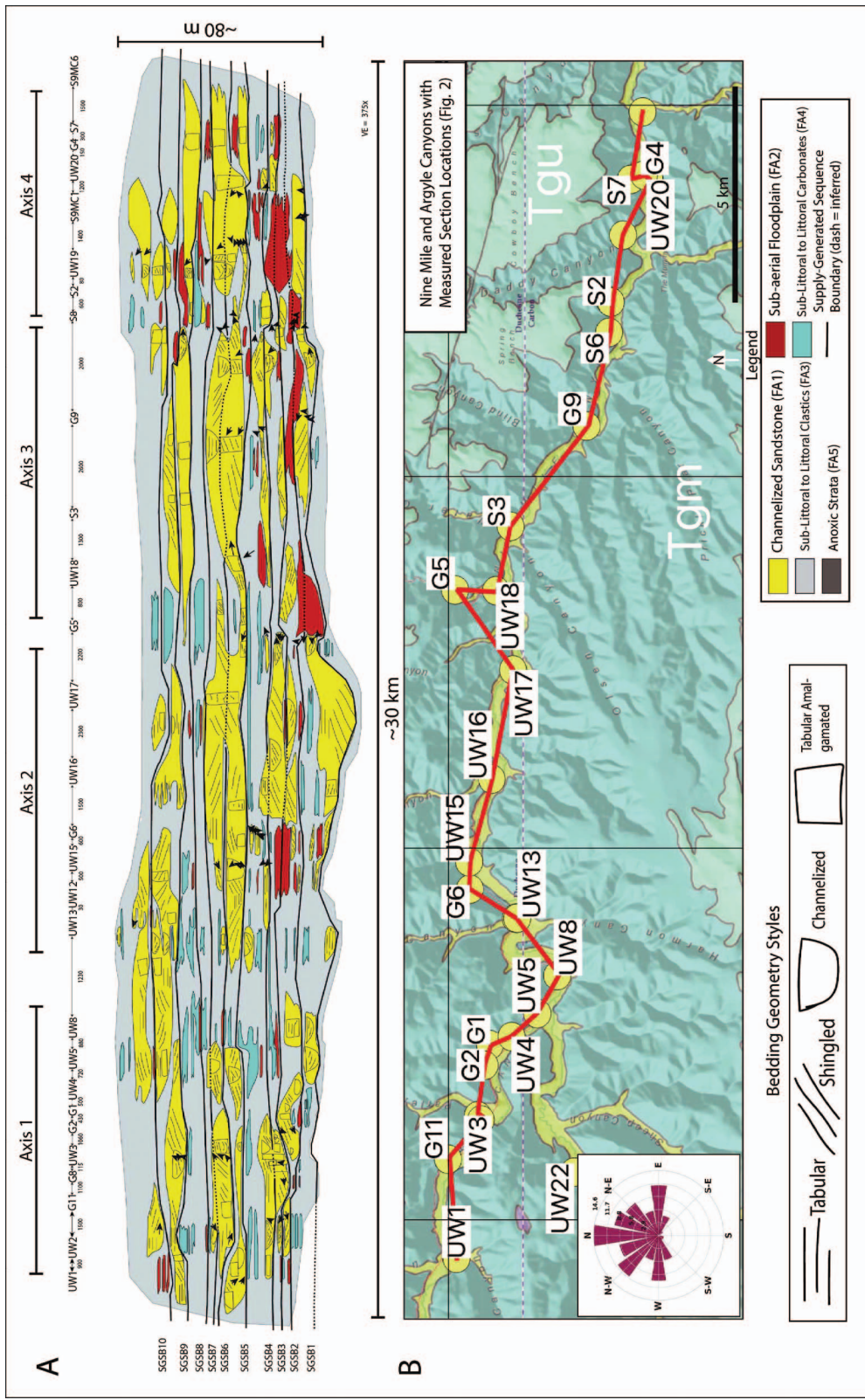


FIG. 10.—Correlation panel of the Sunnyside Interval section of the middle Green River Formation, Uinta Basin, Utah, USA. **A**) Identified facies associations, bedding geometries, paleoflow indicators, and supply-generated sequence boundaries. Log locations with intervening distances are labeled above along with observed lobes of clastic deposition. **B**) Map view of locations of logged sections in Nine Mile and Argyle canyons. Paleoflow measurements are indicated.

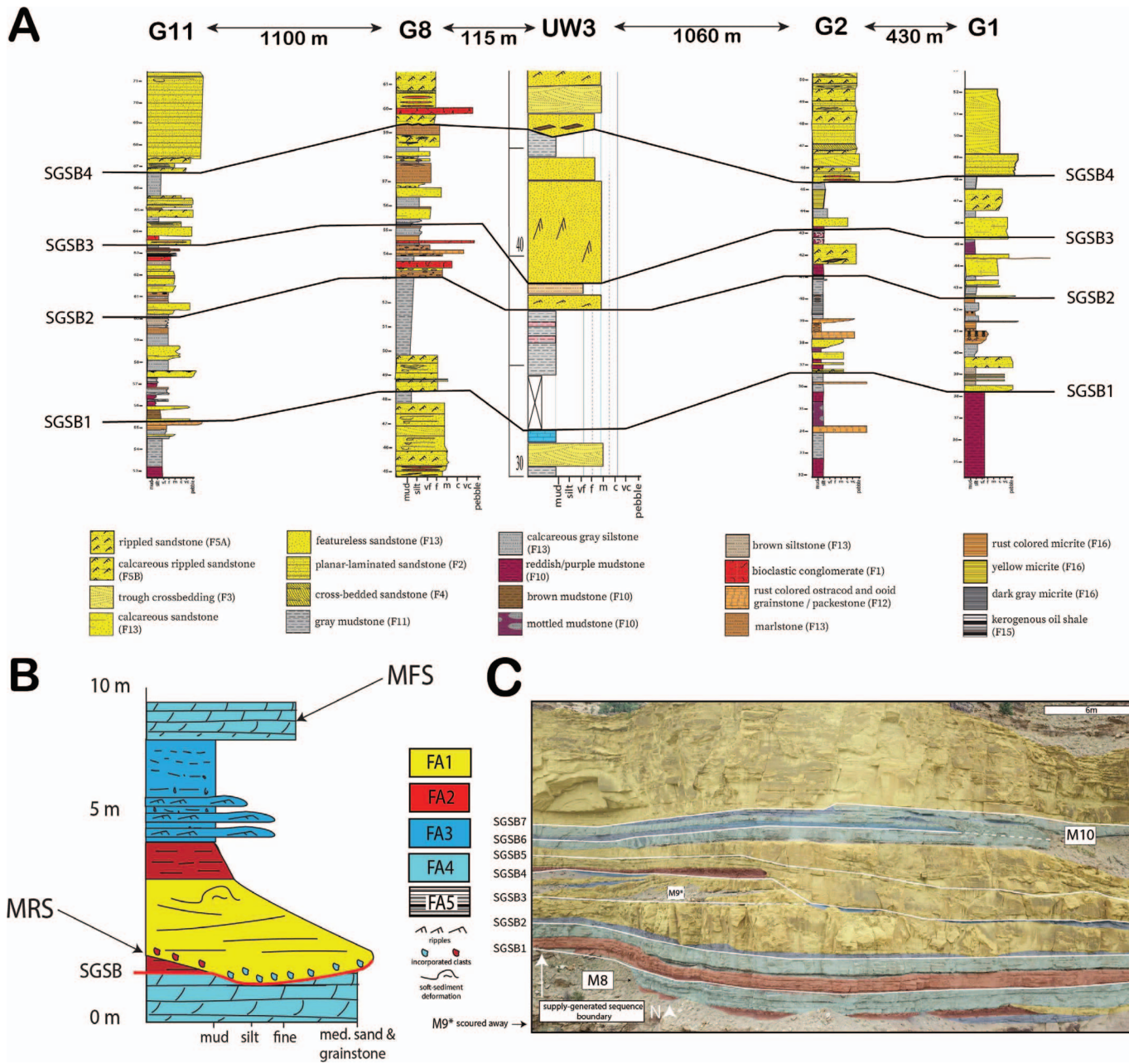


FIG. 11.—Identified and idealized supply-generated sequence architecture. A)  $\sim 2.5$  km correlation of logs G11, G8, UW3 (modified from Remy 1991), G2, and G1. Four supply-generated sequence boundaries are shown subdividing the vertical section into genetic lacustrine sequences based on the SGS methodology. Labeled facies are indicated. B) Idealized form of the supply-generated sequence whereby the SGSB separates facies or surfaces of low-supply from facies of high supply. C) Outcrop illustration showing seven SGSB boundaries located near the mouth of Daddy Canyon with carbonate markers of Keighley et al. (2003).

activity rather than meandering point bars (Wang and Plink-Björklund 2020; Keighley et al. 2021). Facies suggesting extremely variable discharge can be recognized via an abundance of supercritical sedimentary structures (F7), in-channel aggradation and vertical accretion sets, deformed and loaded strata (F8), and in-channel mudstones and mudclasts incorporated into channel sand bodies (F1) (Fielding and Alexander 1996; Wang and Plink-Björklund 2020).

We agree with the variable-discharge interpretation of Sunnyside Interval sandstone deposits (FA1) based on high-velocity bedforms, aggradational channel-fill deposits, and the orientation of shingled bedding styles. Shingled bedding geometries often dip oppositely and obliquely to

one another and display random amounts of lateral overlap between beds (Pusca 2004). In perennial fluvial successions, channel migration and amalgamation generally have a local preferred direction. In such a setting, as was likely in the Sunnyside Interval, any mouth-bar deposits were likely destroyed by prograding channels or sheetfloods or appear thin and widespread when compared with mouth-bar deposits formed in marine basins (Olariu et al. 2021; Keighley et al. 2021).

#### Supply-Generated Sequence Facies Patterns and Stratal Geometries

FA1 units are typically more continuous and abundant just above SGSBs, whereas FA3 units are more abundant and continuous in the

middle of sequences, reflecting a general tendency of deepening water depths during SGS development. Aggradational, pedogenic floodplain deposits (FA2) are most abundant at the base of the SGS, directly on top of SGSBs and sometimes appear conformably inside FA1 channels as mud plugs (Fig. 5C) or laterally as floodplain deposits. Moving up-sequence, littoral to sublittoral clastic deposits (FA3) representing prodeltaic deposition, offshore levees, or near-shore interdistributary-bay deposition overlie and interfinger with the FA1 channelized deposits and FA2 well-drained-floodplain deposits. Littoral to sublittoral carbonates (FA4) appear conformably above the fine-grained clastic deposits of FA3, commonly interfingering laterally and exhibiting gradational contacts throughout the section. FA4 deposits typically exhibit intrasequence upward-shoaling successions and are almost entirely oxidized and commonly desiccated, indicating subaerial exposure (Fig. 7). The rarest facies association, FA5 anoxic strata, makes up the topmost portion of the SGS, appearing below the overlying SGSB. In the Sunnyside Interval FA5 occurs below the SGSB2 and SGSB5 boundaries (Fig. 10A).

In general, sandstone (FA1) bedding geometries (Fig. 9) are distributed variably throughout the transect (except for channelized styles), only showing consistent local trends reflective of genetically related sandstone deposition. Tabular bedding geometries are rarest, generally occurring laterally to other, higher-energy sandstone body styles (channelized and shingled). Shingled and tabular bedding geometries have sharp conformable bedding contacts and little grain-size variability, indicating episodic deposition. Channelized bedding geometries have variable thicknesses within SGSSs but have consistent intra-sequence thickness ranges, from decimeter-scale tabular beds to deposits rarely exceeding 10 m in thickness (Fig. 9). Paleoflow measurements taken from a suite of groove and flute casts, tabular cross-strata, and asymmetric ripples generally record a NNW direction of regional paleoflow but are also highly variable in places (Fig. 10).

The newly defined SGSSs will be referred to as SGS1–SGS10 for clarity. Facies associations (FAs) were assigned to measured-section data (Table 2) within the 10 target sequences (Fig. 10). Taken together, SGS1–SGS10 averages 77 m of section. Divided by 10, each section is approximately 8 m in average thickness. It should be noted that multiple generations of amalgamated channelized deposits (FA1) can destroy easily identifiable SGSBs (Figs. 5D, 9). Sandstone bedding geometries aided in correlating SGSBs throughout the entire correlation panel. Stark vertical changes in bedding-geometry styles indicate temporally distinct depositional events that may have destroyed signals of SGSBs like erosional surfaces, floodplain aggradation, or pedogenic aggradation. Further lines of evidence come from lag deposits (F1) present at the base of thick channelized sandstone deposits (Fig. 4B). The inclusion of clast-rich horizons inside heavily amalgamated sandstone deposits indicates eroded strata representing the very beginning of a given supply-generated sequence.

Lastly, While the term “supply-generated sequence” may appear interpretive in its nomenclature, we argue that since the greater part of the volume of clastic deposition is due to increased riverine discharge in hydrologically closed (endorheic) lakes, the term operates independently of sedimentologic interpretation and should be considered observational if used in similar geologic contexts. Furthermore, even with attempts at standardization, colloquial usage of terms like “sequence boundary” are laden with implicit assumptions about the coupling of sedimentation and base level which is why the “supply-generated” qualifier is used.

## DISCUSSION

### *A Sedimentological Thought Experiment*

To illustrate the logic behind the supply-generated sequence framework, consider an endorheic basin (hydrologically closed), treating groundwater

infiltration and exfiltration as well as aeolian processes as negligible due to poor evidence.

All water outflux from the lake basin is from evaporation (E). Influx comes entirely from precipitation (P) over the catchment area, which is routed to the lake through catchment drainages or captured directly over the surface of the lake.

Clastic sediment primarily comes via riverine discharge. Sources such as landslides and pyroclastic flows are notable exceptions but are not addressed here. Higher values of water discharge correlate with higher values of sediment discharge and increased erosional power (Bohacs et al. 2000; Coe and Birkett 2004; Fisher et al. 2008; Torabi Haghighi and Kløve 2015).

Water can exit the basin, but sediments cannot, thereby leaving a record of basin deposition through time. These strata generally necessitate the existence of a water column (except for pedosols) to explain their deposition and lithification.

For a given catchment, if water influx is larger than outflux ( $P/E > 1$ ), water will accumulate and the lake level will rise. If the opposite is true ( $P/E < 1$ ), water will withdraw and lake level will fall.

If the above precepts are accepted, they imply that the greater part of the volume of clastic deposition in lacustrine sequences occurs during lake-level rise, and therefore lacustrine sequences are generally transgressive in origin. Counterintuitively, these transgressive lacustrine sequences are associated with local aggradation or progradation of the shoreline due to increased riverine discharge and its associated increases in erosion and clastic influx. Following this logic, sequence generation in closed lacustrine systems is stratigraphically *out of phase* compared to marine systems. In other words, the onset of sequence generation is shifted by a half-wavelength in the base-level curve when compared to marine settings (Fig. 12). Bohacs et al. (2000) remarked that lakes are not small oceans. We find, in fact, that they are stratigraphic opposites (Fig. 12).

### *Demonstrated Need for the Supply-Generated-Sequence Model*

The criterion for incorporating a new sequence stratigraphic model must be that the proposed framework provides interpretive utility where others cannot—the Supply-Generated-Sequence Model needs to be substantively different from all other accepted sequence stratigraphic models. The closest established models to the SGS model, in some respects, are the Depositional Sequence II Model of Haq et al. (1987) and Posamentier and Vail (1988), the Genetic Sequence Model of Frazier (1974) and Galloway (1989), and the T-R Sequence Model of Johnson and Murphy (1984) and Embry and Johannessen (1993) (Fig. 13; Catuneanu et al. 2009). The Depositional Sequence II Model places the sequence boundary, a Type I or Type II correlative conformity, at the onset of base-level fall, which is followed by a volumetrically large LST package (Fig. 13). Indeed, this model is predicated on the deposition of thick lowstand fan and wedge deposits during base-level fall, making it unsuitable for closed lacustrine settings (Haq et al. 1987; Posamentier and Vail 1988). The Genetic Sequence Model attempted to de-emphasize Exxonian-style sequence-boundary delineation (e.g., subaerial unconformities) by dividing sequences between maximum flooding surfaces (MFS) identified by thin, condensed marine shale deposits representing rapid base-level rise with little clastic input. The implicit link between condensed-section deposition and base-level rise in the Genetic Sequence Model precludes its use in closed lacustrine systems, where transgressive episodes are associated with large volumes of clastic deposition (Frazier 1974; Galloway 1989). The T-R Sequence Model is conceivably perhaps the “closest” to the proposed SGS model based on the identified sequence boundary (Fig. 13) as a maximum regressive surface (MRS) at the end of regressive episodes (Johnson and Murphy 1984; Embry and Johannessen 1993). The SGSB is not by definition an MRS but will often coincide with the period of maximum regression in closed lakes. This similarity belies what is an

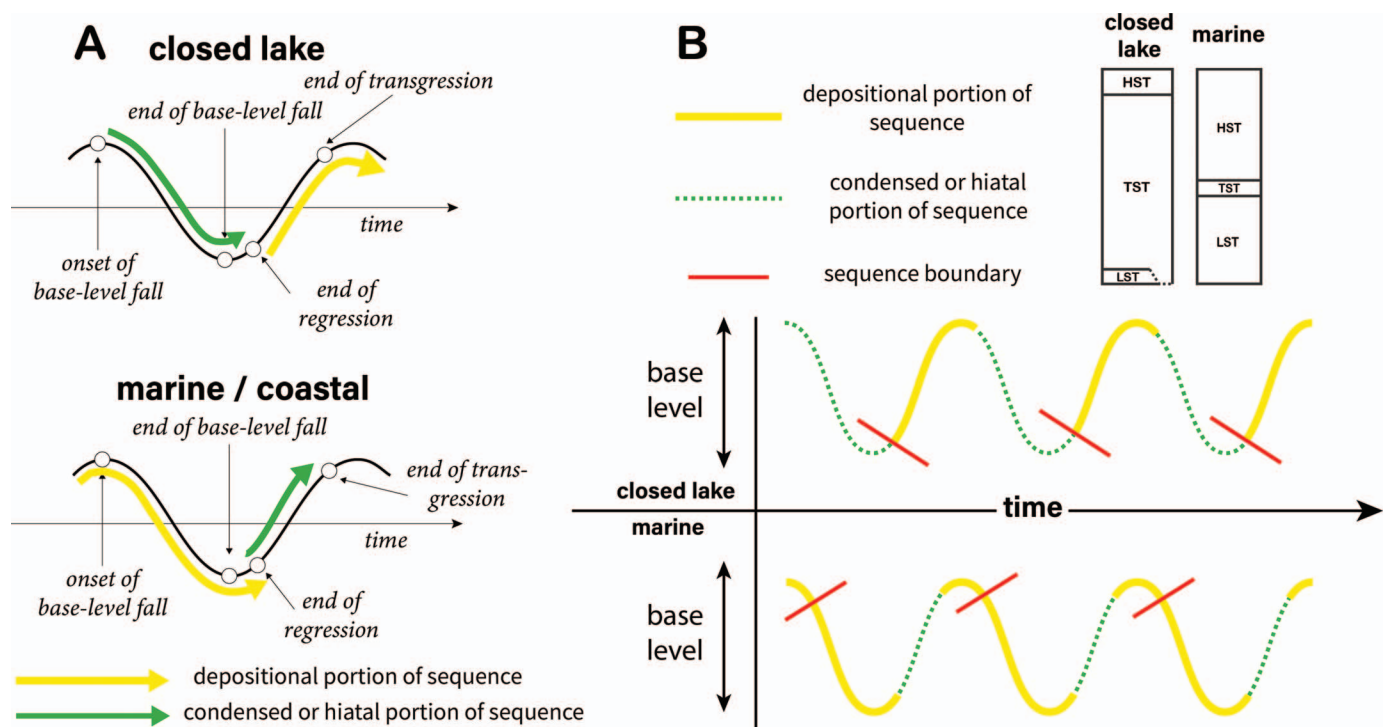


FIG. 12.—The fundamental difference between sequence generation in closed lacustrine vs. marine settings is that the depositional portions of their respective sequences are shifted by a half-wavelength. In other words, the relative volumes of TST and HST-LST strata are opposite. This fact highlights the need for a unified closed lacustrine sequence stratigraphic model. Modified after Catuneanu et al. (2009).

important disparity: that the T-R Sequence Model allows only for regressive and transgressive packages within sequences instead of the higher-resolution HST, LST, TST, divisions. In closed lake systems, the LST is long-lived but quite condensed, sometimes appearing only as signals of subaerial exposure. This stratigraphically minimal package is a crucial portion of the supply-generated sequence in that it is consistent, predictable, and fundamentally distinct from both the HST and TST packages, allowing more precise delineation of sequences and system tracts (Figs. 11–14). This nuance is also the reason to reject the parasequence model of Moore et al. (2012). An additional consideration of the T-R Sequence Model is that it was initially developed for third-order cycles, several orders of magnitude longer in duration than the interpreted Sunnyside Interval sequences.

Creating an exception case within an existing sequence stratigraphic framework for closed lakes would be confusing and unnecessarily complicated due to their unique relationship between base level and sediment supply (Fig. 12). The proposed SGS framework is therefore a distinct sequence stratigraphic model for closed lacustrine settings (Fig. 13).

#### Forcing Mechanisms for Observed Stratigraphy

Recent work has constrained the general timing of the Sunnyside Interval with early Eocene hyperthermal events, and further tied the large FA1 sandstone bodies observed with negative organic carbon isotope excursions, indicating warmer temperatures and more variable seasonal discharges (Birgenheier et al. 2020).

Late Paleocene to Eocene times saw the world in a greenhouse period where temperatures rose to their apex in the Early Eocene Climatic Optimum (EECO). With the rise in global temperatures, transitory hyperthermal events punctuated regional climate through intense, wide-ranging bouts of warming and climatic variability (Thomas and Zachos

2000; Bowen et al. 2006). The hyperthermal events followed orbital forcing schemes, lasting ~40 kyr with hiatuses of 100–400 kyr (Fig. 15). Evidence of increased fluvial deposition during early Eocene hyperthermal events as well as increased carbonate deposition during inter-hyperthermal events can be found in the neighboring Wyoming Green River and Big Horn basins during this same period, indicating global-to-regional climatic events (Abels et al. 2012, 2016; Smith et al. 2014) that resulted in predictable stratigraphic patterns.

Increased precipitation associated with regional climate warming increased both riverine water and sediment discharge, denuding large parts of local topography and deposition into surrounding basins, including the Uinta Basin (Carroll et al. 2006; Smith et al. 2014). Hyperthermal climates in the Uinta Basin are interpreted as semiarid subtropical climate conditions with variable large-scale discharge events (Birgenheier et al. 2020). This interpretation indicates a punctuated equilibrium where short pulses of extreme weather caused high sedimentation rates in semiarid settings dominated by high-flow-regime sedimentary structures (Fig. 15). During inter-hyperthermal periods, clastic and riverine influx was less variable (perennial) but volumetrically smaller than in hyperthermal periods, and the basin margin favored formation of carbonate shoals. At the very beginning of the subsequent hyperthermal event, lake level lowered rapidly due to increasing aridity which occurred quickly compared to the eventual increase in influx of clastics and water (Fig. 15). The existence of this temporally unconfined state of low lake level and low supply is evidenced by the oxidized nature of littoral and sublittoral carbonate deposits during the identified LST portions of the SGS (FA4). As lake level was low and clastic supply had not yet begun to increase, no significant deposition occurred, apart from subaerial-exposure structures in previously deposited strata (Figs. 5, 7). There is further evidence for this period of low-lake-level and low-supply conditions, however: compositions of channel-body lag clasts. The two dominant clast compositions are angular micrite and well-rounded pebbles of varying composition (Fig. 4B).

## Sequence Model Comparisons

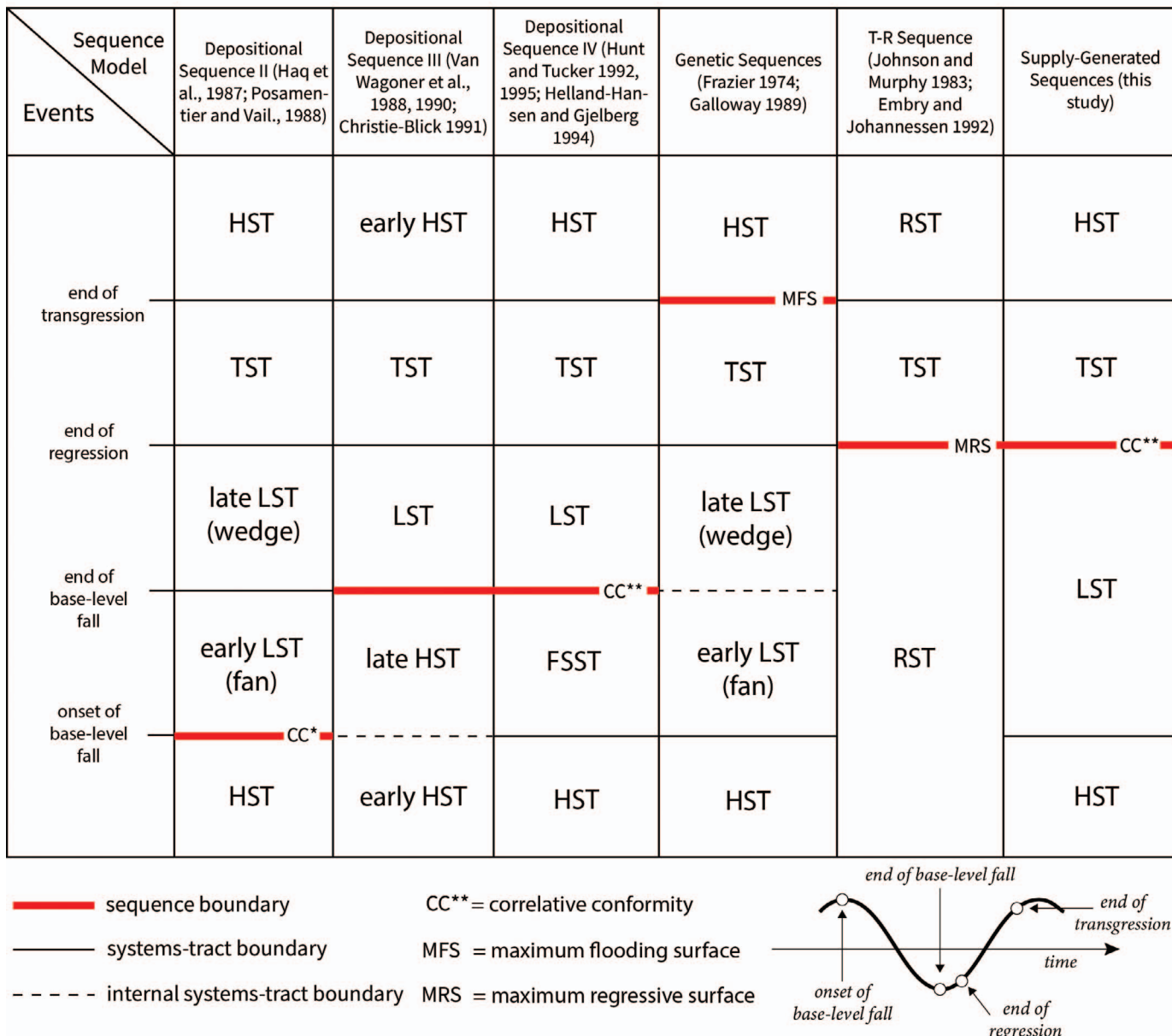


FIG. 13.—The differences in nomenclature, sequence-boundary definition, and systems-tract relationships between classic sequence stratigraphic frameworks and The Supply-Generated-Sequence Model. Modified after Catuneanu et al. (2009).

Evidence from modern semiarid to arid fluvial-lacustrine systems show high degrees of desert-pavement formation. Desert pavements are surfaces topping arid soils in which closely packed, interlocking angular to rounded clasts which can armor the soil's Av horizon over long time periods (4,000–10,000 yr.) (Young et al. 2004). Arid deltas and terminal splays often have interfluves that are armored by pavements. Detailed reports on geomorphology and recent stratigraphy of the Neales Delta in Lake Eyre, Australia, notes the high degree of desert pavements in interfluvial deposits, which may remain dry for years at a time (Hicks 1998). We suggest that the incorporation of these clasts at the bottom of sand bodies (FA1) represents the destruction of armored semiarid to arid soil columns, whereas

incorporation of angular micrites represents incision into exposed littoral to sublittoral carbonate shoals (Fouch 1975).

We present another line of evidence for the Supply-Generated-Sequence Model. Previous workers have dated fossils and tuffs in sections bookending the Sunnyside Interval (Remy 1991; Smith et al. 2008), later compiled and adjusted by Birgenheier et al. (2020), giving a tentative age range of ~1 million years (54–53 Ma) for the Sunnyside Interval. If we consider the 10 sequences of this study making up 40–50% of the Sunnyside Interval (Figs. 3, 14), we can estimate 20–25 sequences existing throughout the entire ~200 m Sunnyside Interval, which have a mean sequence thickness of ~8 m. Dividing 1 Myr by 20–25 gives SGS

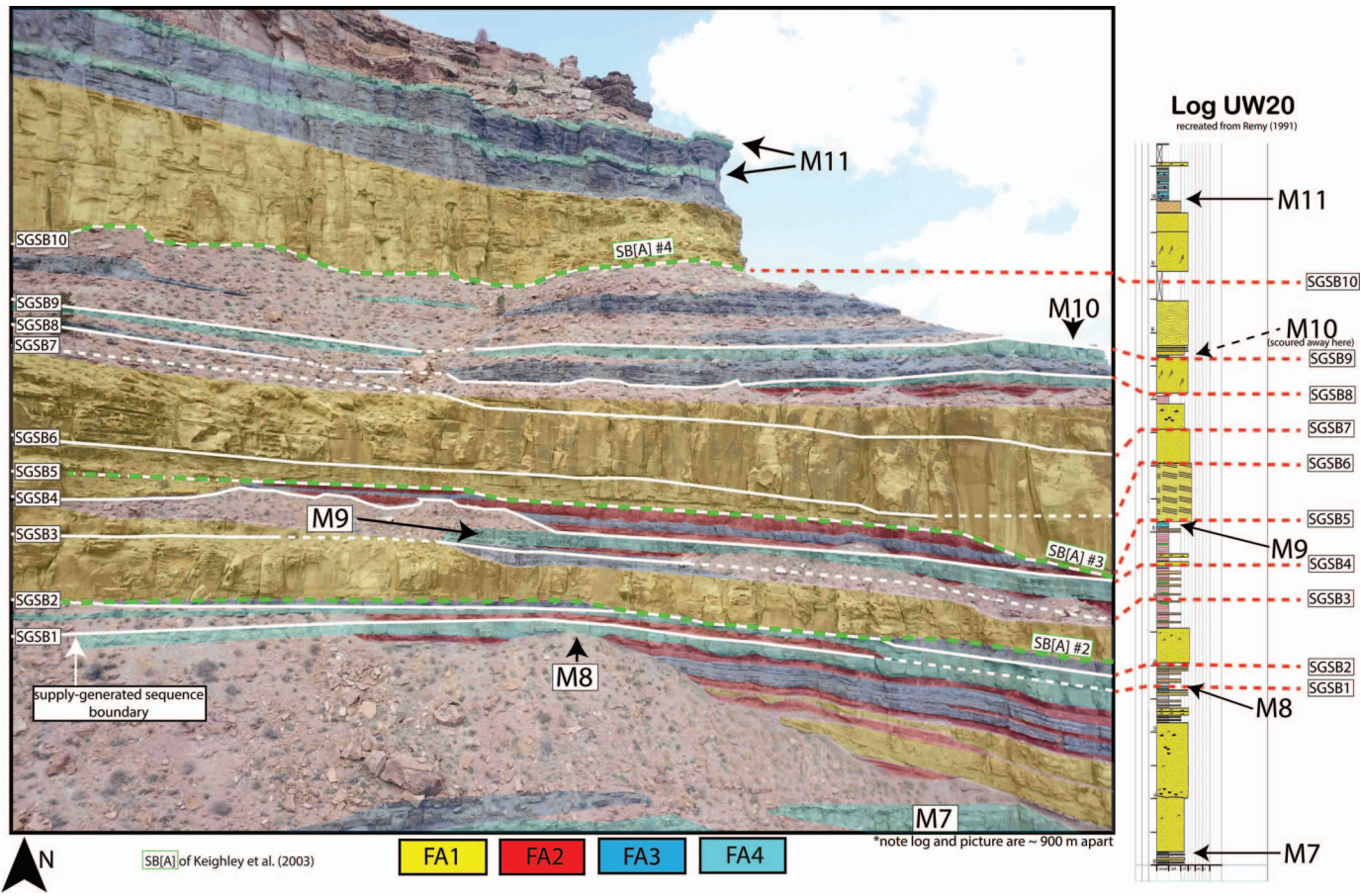


FIG. 14.—Outcrop photo taken near Daddy Canyon correlated with Log UW20 demonstrating the high-resolution afforded by the supply-generated-sequence methodology when compared to previous models. Marker horizons and sequence boundaries of Keighley et al. (2003) are labeled for comparison. Generated with the Supply-Generated-Sequence Model, these SGSBs can be correlated for 30 kilometers along strike.

duration of 40–50 kyr, agreeing well with hyperthermal recurrence times outlined by Birgenheier et al. (2020). This implies that the lake-level HST and TST packages within the SGS are associated with the (relatively) rapid transitory hyperthermals and the LST represents a long period of quiescence (100–400 kyr) during more arid, clastics-starved interhyperthermal times. It should be noted that this is an estimation, but it provides additional support for the SGS model (Fig. 15).

The evidence outlined above corroborates the sediment-supply-controlled nature of the individual Sunnyside Interval SGSs, whereby water discharge and sediment discharge are the controlling factors for creating lacustrine sequences, generating accommodation through lake filling in the form of channelized deposits, terminal splays (FA1 and FA2), and thin prograding and aggrading deltas (Olariu et al. 2021) into a rising-lake-level regime rather than being generated through base-level fall and forced regressions.

Importantly, we do not suggest that climatic drivers are the only forcing mechanism for SGSB creation and SGS development, or that all closed lakes operate under this paradigm—merely that this was the case in Eocene Lake Uinta. As previously mentioned, there may exist an upper volume limit of closed lakes for the applicability of the SGS model. Investigations of lakes in the African Rift System have shown volumetrically large fan deposits associated with lowstand base-level drawdown, indicating a more traditional stratigraphy. Future work is needed to determine whether large and very deep closed lakes can be interpreted accurately using the SGS model. Finally, a schematic idealized depositional model for the Sunnyside

Interval system is presented, displaying deltaic position, morphologies, and generated stratigraphy associated with changes in clastic supply and lake water level (Fig. 15).

## CONCLUSIONS

Here we present the largest known outcrop-based correlation of the Sunnyside Interval fluvio-lacustrine deposits in Nine Mile Canyon near Price, Utah, USA. To subdivide the ~ 30 km, near-depositional-strike correlation panel of the Sunnyside Interval, we applied a novel, unified sequence stratigraphic framework for hydrologically closed lacustrine basins introduced here as the Supply-Generated Sequence Model. The Supply-Generated Sequence Model divides packages of genetic lacustrine strata (supply-generated sequences) by bounding correlative surfaces, conformable or unconformable, separating facies or surfaces associated with low clastic supply (e.g., carbonates, mudstones, or desiccation and exposure surfaces) from facies characteristic of relatively higher amounts of clastic supply (channelized, subaerial sandstones and aggradational pedosols). Using this model, we find that the greatest amount of clastic deposition in closed lakes occurs during lake-level rise, and therefore the supply-generated sequences are characterized as transgressive. This model additionally removes the implicit and explicit base-level assumptions of previous sequence stratigraphic models and accurately captures the “out-of-phase” relationship between lacustrine and marine sequence formation. We further use the supply-generated sequences to argue for a climatic

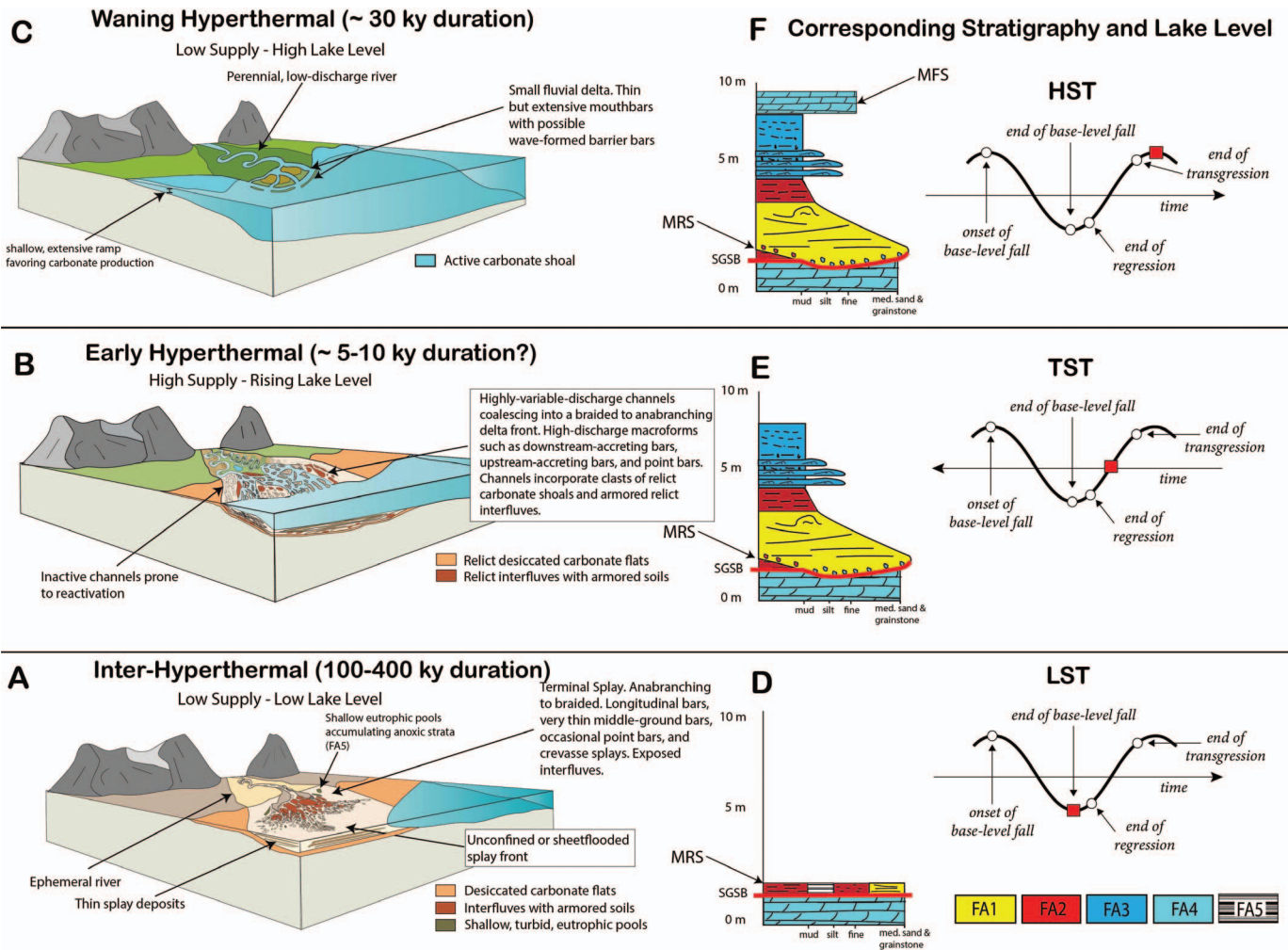


FIG. 15.—A) Schematic model of the Sunnyside Interval depositional system. In stratigraphic order, pairs A and D show the inter-hyperthermal portion of the sequence (LST) which favors anoxic strata and pedogenic aggradation composes the earliest part of the supply-generated sequence (SGS) and is where the maximum regressive surface is located. As the increased catchment water and sediment supply increases during the B) early hyperthermal period, high-discharge channel forms scour into previously deposited strata, sometimes incorporating them into the base of FA1 sandstone deposits (TST). The scour of the FA1 deposit and the base of the aggradational floodplain deposit compose a conformable, time-transgressive boundary indicated a period of increased clastic supply to the basin. As the channel avulses or becomes abandoned a mudplug of well-drained floodplain can form inside the accommodation space created by the erosive channelization of earlier floods. C) As the basin continues to fill with water due to increased riverine discharge, littoral to sublittoral clastic deposits from sheetfloods and/or small deltas conformably overlie the subaerial channel and floodplain strata (HST). Finally, as the hyperthermal wanes and a stable clime of limited sediment discharge arises, the sediment-starved lake begins evaporating, depositing and eventually exposing carbonate shoals (A, LST, FA4).

origin of the cyclic Sunnyside Interval deposits based on cycle frequency aligning with recognized early Eocene transitory hyperthermal events and their associated climatic shifts across the region, increasing riverine discharge of sediment and water. The intermittent nature of these intense depositional events aligns with the strike-variable nature of observed facies and sandstone bedding geometries, representing individual high-magnitude depositional events which eroded and infilled into previous sequences.

#### ACKNOWLEDGMENTS

The authors would like to acknowledge the RioMAR companies for funding, Dr. Brian Horton for his thoughtful comments, John Franey for his fieldwork expertise, and the Dynamic Stratigraphy Group at University of Texas at Austin. Additional thanks go to Tim Hicks and Ed Duncan. We would also like to thank Dr. Janok Bhattacharya for his constructive comments during review.

#### REFERENCES

- ABELS, H.A., CLYDE, W.C., GINGERICH, P.D., HILGEN, F.J., FRICKE, H.C., BOWEN, G.J., AND LOURENS, L.J., 2012, Terrestrial carbon isotope excursions and biotic change during Palaeogene hyperthermals: *Nature Geoscience*, v. 5, p. 326–329, doi:10.1038/ngeo1427.
- ABELS, H.A., LAURETANO, V., VAN YPEREN, A.E., HOPMAN, T., ZACHOS, J.C., LOURENS, L.J., GINGERICH, P.D., AND BOWEN, G.J., 2016, Environmental impact and magnitude of paleosol carbonate carbon isotope excursions marking five early Eocene hyperthermals in the Bighorn Basin, Wyoming: *Climate of the Past*, v. 12, p. 1151–1163, doi:10.5194/cp-12-1151-2016.
- ALLEN, J.P., FIELDING, C.R., RYDEL, M.C., AND GIBLING, M.R., 2013, Deconvolving signals of tectonic and climatic controls from continental basins: an example from the late Paleozoic Cumberland Basin, Atlantic Canada: *Journal of Sedimentary Research*, v. 83, p. 847–872.
- BALÁZS, A., MAGYAR, I., MATENCO, L., SZTANÓ, O., TÓKÉS, L., AND HORVÁTH, F., 2018, Morphology of a large paleo-lake: analysis of compaction in the Miocene–Quaternary Pannonian Basin: *Global and Planetary Change*, v. 171, p. 134–147, doi:10.1016/j.gloplacha.2017.10.012.

- BARTOV, Y., STEIN, M., ENZEL, Y., AGNON, A., AND RECHES, Z., 2002, Lake levels and sequence stratigraphy of Lake Lisan, the late Pleistocene precursor of the Dead Sea: *Quaternary Research*, v. 57, p. 9–21, doi:10.1006/qres.2001.2284.
- BELMONT, P., 2011, Floodplain width adjustments in response to rapid base level fall and knickpoint migration: *Geomorphology*, v. 128, p. 92–102, doi:10.1016/j.geomorph.2010.12.026.
- BIRGENHEIER, L.P., BERG, M.D.V., PLINK-BJÖRKLUND, P., GALL, R.D., ROSENCRANS, E., ROSENBERG, M.J., TOMS, L.C., AND MORRIS, J., 2020, Climate impact on fluvial-lake system evolution, Eocene Green River Formation, Uinta Basin, Utah, USA: *Geological Society of America, Bulletin*, v. 132, p. 562–587, doi:10.1130/B31808.1.
- BLUM, M.D., 1991, Climatic and eustatic controls on gulf coastal plain fluvial sedimentation: an example from the late Quaternary of the Colorado River, Texas, in Armentrout, J.M., and Perkins, B.F., eds., *Sequence Stratigraphy as an Exploration Tool: Concepts and Practices in the Gulf Coast*: SEPM, Gulf Coast Section, v. 11, p. 71–83, doi:10.5724/gcs.90.11.0071.
- BOHACS, K.M., CARROLL, A.R., NEAL, J.E., AND MANKIEWICZ, P.J., 2000, Lake-basin type, source potential, and hydrocarbon character: an integrated sequence-stratigraphic geochemical framework, in Gierlowski-Kordesch, E.H., and Kelts, K.R., eds., *Lake Basins through Space and Time*: American Association of Petroleum Geologists, *Studies in Geology* 46, p. 3–34.
- BOHACS, K.M., CARROLL, A.R., AND NEAL, J.E., 2003, Lessons from large lake systems: thresholds, nonlinearity, and strange attractors, in Chan, M.A., and Archer, A.W., eds., *Extreme Depositional Environments: Mega End Members in Geologic Time*: Geological Society of America, Special Papers, v. 370, p. 75–90.
- BOON, J.J., 1983, Organic geochemical studies of Solar Lake laminated cyanobacterial mats: *Advances in Organic Geochemistry* 1981, p. 207–227.
- BOWEN, G.J., BRALOWER, T.J., DELANEY, M.L., DICKENS, G.R., KELLY, D.C., KOCH, P.L., KUMP, L.R., MENG, J., SLOAN, L.C., THOMAS, E., WING, S.L., AND ZACHOS, J.C., 2006, Eocene hyperthermal event offers insight into greenhouse warming: *American Geophysical Union, Eos, Transactions*, v. 87, p. 165–169, doi:10.1029/2006EO170002.
- BROWN, L.F., AND FISHER, W.L., 1977, Seismic-stratigraphic interpretation of depositional systems: examples from Brazilian rift and pull-apart basins, in Payton, C.E., ed., *Seismic Stratigraphy: Applications to Hydrocarbon Exploration*: American Association of Petroleum Geologists, Memoir 26, p. 213–248, doi:10.1306/M26490C14.
- BURNE, R., AND FERGUSON, J., 1983, Contrasting marginal sediments of a seasonally flooded saline lake: Lake Eliza, South Australia: significance for oil shale genesis: Bureau of Mineral Resources, *Journal of Australian Geology & Geophysics*, v. 8, p. 99–108.
- BUSBY, C., AND INGERSOLL, R.V., 1995, *Tectonics of Sedimentary Basins*: Cambridge, Blackwell Science, 579 p.
- CARROLL, A.R., AND BOHACS, K.M., 1999, Stratigraphic classification of ancient lakes: balancing tectonic and climatic controls: *Geology*, v. 27, p. 99–102, doi:10.1130/0091-7613(1999)027<0099:SCOALB>2.3.CO;2.
- CARROLL, A.R., CHETEL, L.M., AND SMITH, M.E., 2006, Feast to famine: sediment supply control on Laramide basin fill: *Geology*, v. 34, p. 197–200, doi:10.1130/G22148.1.
- CATUNEANU, O., ABREU, V., BHATTACHARYA, J.P., BLUM, M.D., DALRYMPLE, R.W., ERIKSSON, P.G., FIELDING, C.R., FISHER, W.L., GALLOWAY, W.E., GIBLING, M.R., GILES, K.A., HOLBROOK, J.M., JORDAN, R., KENDALL, C.G.S.T.C., MACURDA, B., MARTINSEN, O.J., MIAUL, A.D., NEAL, J.E., NUMMEDAL, D., POMAR, L., POSAMENTER, H.W., PRATT, B.R., SARG, J.F., SHANLEY, K.W., STEEL, R.J., STRASSER, A., TUCKER, M.E., WINKER, C., 2009, Towards the standardization of sequence stratigraphy: *Earth-Science Reviews*, v. 92, p. 1–33, doi:10.1016/j.earscirev.2008.10.003.
- COE, M.T., AND BIRKETT, C.M., 2004, Calculation of river discharge and prediction of lake height from satellite radar altimetry: example for the Lake Chad basin: *Water Resources Research*, v. 40, W10205, doi:10.1029/2003WR002543.
- CROSBY, B.T., AND WHIPPLE, K.X., 2006, Knickpoint initiation and distribution within fluvial networks: 236 waterfalls in the Waipaoa River, North Island, New Zealand: *Geomorphology*, v. 82, p. 16–38, doi:10.1016/j.geomorph.2005.08.023.
- DECELLES, P.G., AND GILES, K.A., 1996, Foreland basin systems: *Basin Research*, v. 8, p. 105–123.
- DICKINSON, W.R., AND SNYDER, W.S., 1978, Plate tectonics of the Laramide orogeny, in Matthews, V. III, ed., *Laramide Folding Associated with Basement Block Faulting in the Western United States*: Geological Society of America, Memoir 151, p. 355–366, doi:10.1130/MEM151-p355.
- DICKINSON, W.R., KLUTE, M.A., HAYES, M.J., JANECKE, S.U., LUNDIN, E.R., McKITTRICK, M.A., AND OLIVARES, M.D., 1988, Paleogeographic and paleotectonic setting of Laramide sedimentary basins in the central Rocky Mountain region: *Geological Society of America, Bulletin*, v. 100, p. 1023–1039, doi:10.1130/0016-7606(1988)100<1023:PAPSO>2.3.CO;2.
- ELJALAFI, A., 2017, Lithofacies, diagenesis, and chemostratigraphy of the microbialite and marginal lacustrine carbonate units within the Green River Formation, eastern Uinta basin, Colorado and Utah [Ph.D. Thesis]: Colorado School of Mines, 137 p.
- EMBRY, A.F., AND JOHANNESSEN, E.P., 1993, T-R sequence stratigraphy, facies analysis and reservoir distribution in the uppermost Triassic–Lower Jurassic succession, western Sverdrup Basin, Arctic Canada, in Vorren, T.O., Bergsager, E., Dahl-Stamnes, Ø.A., Holter, E., Johansen, B., Lie, E., and Lund, T.B., eds., *Arctic Geology and Petroleum Potential*: Norwegian Petroleum Society, Special Publication 2, p. 121–146, doi:10.1016/B978-0-444-88943-5.00013-7.
- FAN, M., AND CARRAPA, B., 2014, Late Cretaceous–early Eocene Laramide uplift, exhumation, and basin subsidence in Wyoming: crustal responses to flat slab subduction: Laramide uplift and exhumation: *Tectonics*, v. 33, p. 509–529, doi:10.1002/2012TC003221.
- FENG, Y., LI, S., AND LU, Y., 2013, Sequence stratigraphy and architectural variability in Late Eocene lacustrine strata of the Dongying Depression, Bohai Bay Basin, Eastern China: *Sedimentary Geology*, v. 295, p. 1–26, doi:10.1016/j.sedgeo.2013.07.004.
- FENG, Y., JIANG, S., HU, S., LI, S., LIN, C., AND XIE, X., 2016, Sequence stratigraphy and importance of syndepositional structural slope-break for architecture of Paleogene synrift lacustrine strata, Bohai Bay Basin, E. China: *Marine and Petroleum Geology*, v. 69, p. 183–204, doi:10.1016/j.marpetgeo.2015.10.013.
- FIELDING, C.R., AND ALEXANDER, J., 1996, Sedimentology of the Upper Burdekin River of North Queensland, Australia: an example of a tropical, variable discharge river: *Terra Nova*, v. 8, p. 447–457, doi:10.1111/j.1365-3121.1996.tb00770.x.
- FISHER, J.A., KRAPE, C.B.E., LANG, S.C., NICHOLS, G.J., AND PAYENBERG, T.H.D., 2008, Sedimentology and architecture of the Douglas Creek terminal splay, Lake Eyre, central Australia: *Sedimentology*, v. 55, p. 1915–1930, doi:10.1111/j.1365-3091.2008.00974.x.
- FONGNGERN, R., OLARIU, C., STEEL, R., MOHRIG, D., KRÉZEK, C., AND HESS, T., 2018, Subsurface and outcrop characteristics of fluvial-dominated deep-lacustrine clinoforms: *Sedimentology*, v. 65, p. 1447–1481, doi:10.1111/sed.12430.
- FOUCH, T.D., 1975, Lithofacies and related hydrocarbon accumulations in Tertiary strata of the western and central Uinta Basin, Utah, in Boldyard, D.W., ed., *Symposium on Deep Drilling Frontiers of the Central Rocky Mountains*: Rocky Mountain Association of Geologists, p. 163–173.
- FRAZIER, D.E., 1974, Depositional Episodes: Their Relationship to the Quaternary Stratigraphic Framework in the Northwestern Portion of the Gulf Basin: The University of Texas at Austin, Bureau of Economic Geology, Geological Circular 74-1, 28 p.
- GALL, R.D., BIRGENHEIER, L.P., AND VANDEN BERG, M.D., 2017, Highly seasonal and perennial fluvial facies: implications for climatic control on the Douglas Creek and Parachute Creek members, Green River Formation, southeastern Uinta Basin, Utah, U.S.A.: *Journal of Sedimentary Research*, v. 87, p. 1019–1047, doi:10.2110/jsr.2017.54.
- GALLOWAY, W.E., 1989, Genetic stratigraphic sequences in basin analysis I: architecture and genesis of flooding-surface bounded depositional units: *American Association of Petroleum Geologists, Bulletin*, v. 73, p. 125–142, doi:10.1306/703C9AF5-1707-11D7-8645000102C1865D.
- GÖNG, C., SZTANÓ, O., STEEL, R.J., XIAN, B., GALLOWAY, W.E., AND BADA, G., 2019, Critical differences in sediment delivery and partitioning between marine and lacustrine basins: a comparison of marine and lacustrine aggradational to progradational clinoform pairs: *Geological Society of America, Bulletin*, v. 131, p. 766–781, doi:10.1130/B32042.1.
- HAGHIGHI, A.T., AND KLOVE, B., 2015, A sensitivity analysis of lake water level response to changes in climate and river regimes: *Limnologica*, v. 51, p. 118–130, doi:10.1016/j.limno.2015.02.001.
- HAQ, B.U., HARDENBOL, J., AND VAIL, P.R., 1987, Chronology of fluctuating sea levels since the Triassic: *Science*, v. 235, p. 1156–1167, doi:10.1126/science.235.4793.1156.
- HECKY, R.E., AND KILHAM, P., 1973, Diatoms in alkaline, saline lakes: ecology and geochemical implications: *Limnology and Oceanography*, v. 18, p. 53–71, doi:10.4319/lo.1973.18.1.00053.
- HELLAND-HANSEN, W., AND GJELBERG, J.G., 1994, Conceptual basis and variability in sequence stratigraphy: a different perspective: *Sedimentary Geology*, v. 92, p. 31–52, doi:10.1016/0037-0738(94)90053-1.
- HICKS, T., 1998, Stratigraphy, reservoir geometry and facies architecture of a modern arid playa basin lacustrine delta: Neales River Delta, Lake Eyre, Australia [BAThesis]: Queensland University of Technology, p. 60–64.
- HOOGENDOORN, R.M., BOELS, J.F., KROONENBERG, S.B., SIMMONS, M.D., ALIYEVA, E., BABAZADEH, A.D., AND HUSEYNOV, D., 2005, Development of the Kura delta, Azerbaijan: a record of Holocene Caspian sea-level changes: *Marine Geology*, v. 222, p. 359–380.
- HORTON, B.K., YIN, A., SPURLIN, M.S., ZHOU, J., AND WANG, J., 2002, Paleocene–Eocene syncontractional sedimentation in narrow, lacustrine-dominated basins of east-central Tibet: *Geological Society of America, Bulletin*, v. 114, p. 771–786.
- HUNT, D., AND TUCKER, M.E., 1992, Standard parasequences and the forced regressive wedge system tract: deposition during base level fall: *Sedimentary Geology*, v. 81, p. 1–9, doi:10.1016/0037-0738(92)90052-S.
- HUYBERS, K., RUPPER, S., AND ROE, G.H., 2016, Response of closed basin lakes to interannual climate variability: *Climate Dynamics*, v. 46, p. 3709–3723, doi:10.1007/s00382-015-2798-4.
- ILGAR, A., AND NEMEC, W., 2005, Early Miocene lacustrine deposits and sequence stratigraphy of the Ermenek Basin, Central Taurides, Turkey: *Sedimentary Geology*, v. 173, p. 233–275, doi:10.1016/j.sedgeo.2003.07.007.
- JACKSON, L.J., 2003, Macrophyte-dominated and turbid states of shallow lakes: evidence from Alberta Lakes: *Ecosystems*, v. 6, p. 213–223, doi:10.1007/s10021-002-0001-3.
- JACOB, A., 1969, Delta facies of the Green River Formation (Eocene), Carbon and Duchesne counties, Utah [Ph.D. Thesis]: University of Colorado, 97 p.
- JOHNSON, J.G., AND MURPHY, M.A., 1984, Time–rock model for Silurian–Devonian continental shelf, western United States: *Geological Society of America, Bulletin*, v. 95, p. 1349–1359, doi:10.1130/0016-7606(1984)95<1349:TMFSCS>2.0.CO;2.
- JOHNSON, R.C., 1985, Early Cenozoic history of the Uinta and Piceance Creek basins, Utah and Colorado, with special reference to the development of Eocene Lake Uinta: in Flores, R.M., and Kaplan, S.S., eds., *Cenozoic Paleogeography of the West-Central United States*: SEPM, Rocky Mountain Section, p. 247–276.
- JORISSEN, E.L., ABELS, H.A., WESSELINGH, F.P., LAZAREV, S., AGHAYEVA, V., AND KRIJGSMA, W., 2020, Amplitude, frequency and drivers of Caspian Sea lake-level variations during

- the Early Pleistocene and their impact on a protected wave-dominated coastline: *Sedimentology*, v. 67, p. 649–676, doi:10.1111/sed.12658.
- KEIGHLEY, D.G., AND FLINT, S.S., 2008, Fluvial sandbody geometry and connectivity in the middle Green River Formation, Nine Mile Canyon, southwestern Uinta Basin, in Longman, M.W., and Morgan, C.D., eds., *Hydrocarbon Systems and Production in the Uinta Basin, Utah*, Rocky Mountain Association of Geologists and Utah Geological Association, Publication 37, p. 101–120.
- KEIGHLEY, D., FLINT, S., HOWELL, J., ANDERSON, D., COLLINS, S., MOSCARELLO, A., AND STONE, G., 2002, Surface and Subsurface Correlation of the Green River Formation in Central Nine Mile Canyon, SW Uinta Basin Carbon and Duchesne Counties, East-Central Utah: Utah Geological Survey, MP-02-01, 63 p.
- KEIGHLEY, D., FLINT, S., HOWELL, J., AND MOSCARELLO, A., 2003, Sequence Stratigraphy in Lacustrine Basins: A Model for Part of the Green River Formation (Eocene), southwest Uinta Basin, Utah, U.S.A.: *Journal of Sedimentary Research*, v. 73, p. 987–1006, doi:10.1306/050103730987.
- KEIGHLEY, D., SPINNANGR, Ø., HOWELL, J., AND FLINT, S., 2021, Interpretation of mouth-bar and related lacustrine and fluvial sand bodies from the middle Green River Formation (Eocene), southern Uinta Basin, Utah, in Starratt, S.W., and Rosen, M.R., eds., *From Saline to Freshwater: The Diversity of Western Lakes in Space and Time: Geological Society of America, Special Paper 536*, p. 259–287, doi:10.1130/2019.2536(15).
- KNOX, J.C., 1975, Concept of the graded stream, in Melhorn, W.N., and Flemal, R.C., eds., *Theories of Landform Development*: State University of New York, Binghamton, Geomorphology Symposia Series, p. 169–198.
- KOENINGS, J.P., AND EDMUNDSON, J.A., 1991, Secchi disk and photometer estimates of light regimes in Alaskan lakes: effects of yellow color and turbidity: *Limnology and Oceanography*, v. 36, p. 91–105, doi:10.4319/lo.1991.36.1.0091.
- KUMAR, R., 1993, Coalescence megafan: multistory sandstone complex of the late-orogenic (Mio-Pliocene) sub-Himalayan belt, Dehra Dun, India: *Sedimentary Geology*, v. 85, p. 327–337.
- LASKE, G., AND MASTERS, G., 1997, A global digital map of sediment thickness: American Geophysical Union, Eos, Transactions, v. 78, F483.
- LAWTON, T.F., 2019, Laramide sedimentary basins and sediment-dispersal systems, in Miall, A.D., ed., *The Sedimentary Basins of the United States and Canada*: Elsevier, p. 529–557, doi:10.1016/B978-0-444-63895-3.00013-9.
- LEMONS, D.R., AND CHAN, M.A., 1999, Facies architecture and sequence stratigraphy of fine-grained lacustrine deltas along the eastern margin of late Pleistocene Lake Bonneville, northern Utah and southern Idaho: American Association of Petroleum Geologists, *Bulletin*, v. 83, p. 635–665, doi:10.1306/00AA9C14-1730-11D7-8645000102C1865D.
- MCKEE, E.D., 1965, Experiments in ripple lamination, in Middleton, G.V., ed., *Primary sedimentary structures and their hydrodynamic interpretation*: SEPM, Special Publication 12, p. 66–83.
- MILLIGAN, M.R., AND CHAN, M.A., 1998, Coarse-grained Gilbert deltas: facies, sequence stratigraphy and relationships to Pleistocene climate at the eastern margin of Lake Bonneville, northern Utah, in Kocurek, G., ed., *Relative Role of Eustasy, Climate, and Tectonism in Continental Rocks: SEPM*, v. 59, p. 177–189, doi:10.2110/pec.98.59.0176.
- MITCHUM, R.M., AND VAN WAGONER, J.C., 1991, High-frequency sequences and their stacking patterns: sequence-stratigraphic evidence of high-frequency eustatic cycles: *Sedimentary Geology*, v. 70, p. 131–160, doi:10.1016/0037-0738(91)90139-5.
- MOORE, J., TAYLOR, A., JOHNSON, C., RITTS, B.D., AND ARCHER, R., 2012, Facies analysis, reservoir characterization, and LIDAR modeling of an Eocene lacustrine delta, Green River Formation, southwest Uinta basin, Utah, in Baganz, O.W., Bartov, Y., Bohacs, K., and Nummedal, D., eds., *Lacustrine Sandstone Reservoirs and Hydrocarbon Systems*: American Association of Petroleum Geologists, Memoir 95, p. 183–208, doi:10.1306/6/13291389M953449.
- MORGAN, C.D., AND BERESKIN, S.R., 2003, Characterization of Petroleum Reservoirs in the Eocene Green River Formation, central Uinta Basin, Utah: *The Mountain Geologist*, Rocky Mountain Association of Geologists, v. 39, p. 111–127.
- NEAL, J., AND ABREU, V., 2009, Sequence stratigraphy hierarchy and the accommodation succession method: *Geology*, v. 37, p. 779–782.
- NUTZ, A., SCHUSTER, M., BOËS, X., AND RUBINO, J.-L., 2017, Orbitally-driven evolution of Lake Turkana (Turkana Depression, Kenya, EARS) between 1.95 and 1.72 Ma: a sequence stratigraphy perspective: *Journal of African Earth Sciences*, v. 125, p. 230–243, doi:10.1016/j.jafrearsci.2016.10.016.
- NUTZ, A., SCHUSTER, M., BARBONI, D., GASSIER, G., VAN BOXLAEER, B., ROBIN, C., RAGON, T., GHENNE, J.-F., AND RUBINO, J.-L., 2020, Plio-Pleistocene sedimentation in West Turkana (Turkana Depression, Kenya, East African Rift System): paleolake fluctuations, paleolandscapes and controlling factors: *Earth-Science Reviews*, v. 211, no. 103415, doi:10.1016/j.earscirev.2020.103415.
- OLARIU, C., ZHOU, C., STEEL, R., ZHANG, Z., YUAN, X., ZHANG, J., CHEN, S., CHENG, D., AND KIM, W., 2021, Controls on the stratal architecture of lacustrine delta successions in low-accommodation conditions: *Sedimentology*, v. 68, p. 1941–1963, doi:10.1111/sed.12838.
- OLSEN, H., 1989, Sandstone-body structures and ephemeral stream processes in the Dinosaur Canyon Member, Moenave Formation (Lower Jurassic), Utah, U.S.A.: *Sedimentary Geology*, v. 61, p. 207–221, doi:10.1016/0037-0738(89)90058-4.
- OEVEREM, I., KROONENBERG, S.B., VELDKAMP, A., GROENESTEIJN, K., RUSAKOV, G.V., AND SVITOCH, A.A., 2003, Small-scale stratigraphy in a large ramp delta: recent and Holocene sedimentation in the Volga delta, Caspian Sea: *Sedimentary Geology*, v. 159, p. 133–157, doi:10.1016/S0037-0738(02)00256-7.
- POSAMENTIER, H.W., AND VAIL, P.R., 1988, Eustatic controls on clastic deposition II: sequence and systems tract models, in Wilgus, C.K., Hastings, B.S., Posamentier, H., Van Wagoner, J., Ross, C.A., and Kendall, C.G.St.C., eds., *Sea-Level Changes: An Integrated Approach: SEPM, Special Publication 42*, p. 125–154, doi:10.2110/pec.88.01.0125.
- PUSCA, V.A., 2004, Wet/dry, terminal fan-dominated sequence architecture: a new, outcrop-based model for the lower Green River Formation, Utah [Ph.D. Thesis]: University of Wyoming, 181 p.
- REMY, R.R., 1991, Analysis of Lacustrine Deltaic Sedimentation in the Green River Formation, Southern Uinta Basin, Utah. (Volumes I and II) [Ph.D. Thesis]: Louisiana State University, 484 p.
- RIDING, R., 2011, The nature of stromatolites: 3,500 million years of history and a century of research, in Reitner, J., Quéric, N., and Arp, G., eds., *Advances in Stromatolite Geobiology: Lecture Notes in Earth Sciences*, v. 131, p. 29–74, doi:10.1007/978-3-642-10415-2\_3.
- RUBLE, T.E., LEWAN, M.D., AND PHILP, R.P., 2001, New insights on the green river petroleum system in the Uinta Basin from hydrous pyrolysis experiments: *American Association of Petroleum Geologists, Bulletin*, v. 85, p. 1333–1371, doi:10.1306/8626CAB9-173B-11D7-8645000102C1865D.
- RYDER, R.T., FOUCHE, T.D., AND ELISON, J.H., 1976, Early Tertiary sedimentation in the western Uinta basin, Utah: *Geological Society of America, Bulletin*, v. 87, p. 496–512.
- SCHOMACKER, E.R., KJEMPERUD, A.V., NYSTUEN, J.P., AND JAHREN, J.S., 2010, Recognition and significance of sharp-based mouth-bar deposits in the Eocene Green River Formation, Uinta Basin, Utah: Green River Formation mouth-bar deposits: *Sedimentology*, v. 57, p. 1069–1087, doi:10.1111/j.1365-3091.2009.01136.x.
- SHANLEY, K.W., AND McCABE, P.J., 1994, Perspectives on the sequence stratigraphy of continental strata: *American Association of Petroleum Geologists, Bulletin*, v. 78, p. 544–568, doi:10.1306/BDFF9258-1718-11D7-8645000102C1865D.
- SMITH, M.E., CARROLL, A.R., AND SINGER, B.S., 2008, Synoptic reconstruction of a major ancient lake system: Eocene Green River Formation, western United States: *Geological Society of America, Bulletin*, v. 120, p. 54–84.
- SMITH, M.E., CARROLL, A.R., SCOTT, J.J., AND SINGER, B.S., 2014, Early Eocene carbon isotope excursions and landscape destabilization at eccentricity minima: Green River Formation of Wyoming: *Earth and Planetary Science Letters*, v. 403, p. 393–406, doi:10.1016/j.epsl.2014.06.024.
- SPINNANGR, Ø., 2014, *Sedimentology and Geometry of Fluvial and Deltaic Sandbodies in the Eocene Green River Formation, Eastern Utah* [MS Thesis]: University of Bergen, 142 p.
- STANLEY, K.O., AND COLLINSON, J.W., 1979, Depositional history of Paleocene–Lower Eocene Flagstaff Limestone and coeval rocks, central Utah: *American Association of Petroleum Geologists, Bulletin*, v. 63, p. 311–323, doi:10.1306/C1EA5602-16C9-11D7-8645000102C1865D.
- STEAR, W.M., 1985, Comparison of the bedform distribution and dynamics of modern and ancient sandy ephemeral flood deposits in the southwestern Karoo region, South Africa: *Sedimentary Geology*, v. 45, p. 209–230, doi:10.1016/0037-0738(85)90003-X.
- TĀNAVSUU-MILKEVICIENE, K., SARG, J.F., AND BARTOV, Y., 2017, Depositional cycles and sequences in an organic-rich lake basin: Eocene Green River Formation, Lake Uinta, Colorado and Utah, U.S.A.: *Journal of Sedimentary Research*, v. 87, p. 210–229, doi:10.2110/jstr.2017.11.
- TAYLOR, A.W., AND RITTS, B.D., 2004, Mesoscale heterogeneity of fluvial–lacustrine reservoir analogues: examples from the Eocene Green River and Colton formations, Uinta Basin, Utah, USA: *Journal of Petroleum Geology*, v. 27, p. 3–26.
- THOMAS, E., AND ZACHOS, J.C., 2000, Was the late Paleocene thermal maximum a unique event? *Geological Society of Sweden, Journal*, v. 122, p. 169–170, doi:10.1080/11035890001221169.
- TŌRŌ, B., AND PRATT, B.R., 2015, Characteristics and implications of sedimentary deformation features in the Green River Formation (Eocene) in Utah and Colorado, in Vanden Berg, M.D., Ressetar, R., and Birgenheier, L.P., eds., *Geology of Utah's Uinta Basin and Uinta Mountains: Utah Geological Association, Publication 44*, p. 371–422.
- TUNBRIDGE, I.P., 1981, Sandy high-energy flood sedimentation: some criteria for recognition, with an example from the Devonian of S.W. England: *Sedimentary Geology*, v. 28, p. 79–95, doi:10.1016/0037-0738(81)90058-0.
- VAIL, P.R., MITCHUM, R.M., JR., AND THOMPSON, S., III, 1977, Seismic stratigraphy and global changes of sea level, part 4: global cycles of relative changes of sea level, in Payton, C.E., ed., *Seismic Stratigraphy: Applications to Hydrocarbon Exploration*: American Association of Petroleum Geologists, Memoir 26 p. 86–97.
- VAN DEN BERG, J.H., AND VAN GELDER, A., 1993, Prediction of suspended bed material transport in flows over silt and very fine sand: *Water Resources Research*, v. 29, p. 1393–1404, doi:10.1029/92WR02654.
- VAN WAGONER, J.C., POSAMENTIER, H.W., MITCHUM, R.M., JR., VAIL, P.R., SARG, J.F., LOUTIT, T.S., AND HARDENBOL, J., 1988, An overview of the fundamentals of sequence stratigraphy and key definitions, in Wilgus, C.K., Hastings, B.S., Posamentier, H., Van Wagoner, J., Ross, C.A., and Kendall, C.G.St.C., *Sea-Level Changes: An Integrated Approach: SEPM, Special Publication 42*, doi:10.2110/pec.88.01.0039.
- VAN WAGONER, J.C., MITCHUM, R.M., CAMPION, K.M., AND RAHMANIAN, V.D., 1990, Siliciclastic Sequence Stratigraphy in Well Logs, Cores, and Outcrops: Concepts for

- High-Resolution Correlation of Time and Facies: American Association of Petroleum Geologists, v. 7, 60 p., doi:10.1306/Mth7510.
- WANG, J., PLINK-BJÖRKLUND, P., 2019, Stratigraphic complexity in fluvial fans: Lower Eocene Green River Formation, Uinta Basin, USA: *Basin Research*, v. 31, p. 892–919, doi:10.1111/bre.12350.
- WANG, J., AND PLINK-BJÖRKLUND, P., 2020, Variable-discharge-river macroforms in the Sunnyside Delta interval of the Eocene Green River Formation, Uinta Basin, USA: *Sedimentology*, v. 67, p. 1914–1950, doi:10.1111/sed.12688.
- YOUNG, M.H., McDONALD, E.V., CALDWELL, T.G., BENNER, S.G., AND MEADOWS, D.G., 2004, Hydraulic properties of a desert soil chronosequence in the Mojave Desert, USA: *Vadose Zone Journal*, v. 3, p. 956–963.
- ZALEHA, M.J., 1997, Intra- and extrabasinal controls on fluvial deposition in the Miocene Indo-Gangetic foreland basin, northern Pakistan: *Sedimentology*, v. 44, p. 369–390, doi:10.1111/j.1365-3091.1997.tb01530.x
- ZHANG, J., OLARIU, C., STEEL, R., AND KIM, W., 2020, Climatically controlled lacustrine clinoforms: theory and modelling results: *Basin Research*, v. 32, p. 240–250, doi:10.1111/bre.12383.
- ZOU, C., ZHANG, X., LUO, P., WANG, L., LIU, Z., AND LIU, L., 2010, Shallow-lacustrine sand-rich deltaic depositional cycles and sequence stratigraphy of the Upper Triassic Yanchang Formation, Ordos Basin, China: *Basin Research*, v. 22, p. 108–125, doi:10.1111/j.1365-2117.2009.00450.x.

Received 9 August 2021; accepted 2 June 2022.